UNDERSTANDING GRANULAR MATERIALS BY THEIR FORCE NETWORKS

by

JAMES SARTOR

A DISSERTATION

Presented to the Department of Physics
and the Division of Graduate Studies of the University of Oregon
in partial fulfillment of the requirements
for the degree of
Doctor of Philosophy

December 2021

DISSERTATION APPROVAL PAGE

Student: James Sartor

Title: Understanding Granular Materials by Their Force Networks

This dissertation has been accepted and approved in partial fulfillment of the requirements for the Doctor of Philosophy degree in the Department of Physics by:

Ben Mcmorran	Chair
Eric Corwin	Advisor
Jayson Paulose	Core Member
Marina Guenza	Institutional Representative

and

Andy Karduna	Interim Vice Provost for Graduate Studies

Original approval signatures are on file with the University of Oregon Division of Graduate Studies.

Degree awarded December 2021

DISSERTATION ABSTRACT

James Sartor

Doctor of Philosophy

Department of Physics

December 2021

Title: Understanding Granular Materials by Their Force Networks

abstract here

This dissertation includes previously published and unpublished coauthored material.

CURRICULUM VITAE

NAME OF AUTHOR: James Sartor

GRADUATE AND UNDERGRADUATE SCHOOLS ATTENDED:

University of Oregon, Eugene, OR, USA
Auburn University, Auburn, AL, USA

DEGREES AWARDED:

Doctor of Philosophy, Physics, 2021, University of Oregon
Master of Science, Physics, 2017, University of Oregon
Bachelor of Science, Department of Physics, Physics, 2013, Auburn University

AREAS OF SPECIAL INTEREST:

Soft Condensed Matter, Jamming

PROFESSIONAL EXPERIENCE:

Graduate Employee, University of Oregon, 2016-2021

Software Developer, Performance Logic 2014-2015

Undergraduate Research Assistant, Auburn University 2011-2014

GRANTS, AWARDS AND HONORS:

Weiser Senior Teaching Assistant Award, UO Department of Physics, 2021

PUBLICATIONS:

J. Sartor, and E.I. Corwin, "Predicting Defects in Soft Sphere Packings Near Jamming Using The Force Network Ensemble" *arxiv preprint* arXiv:2108.09385 (2021).

J. Sartor, S. A. Ridout, and E. I. Corwin, "Mean-Field Predictions of Scaling Prefactors Match Low-Dimensional Jammed Packings" *Phys Rev Letters* **126** (4) 048001 (2021)

J. Sartor and E. I. Corwin, "Direct measurement of force configurational entropy in jamming" *Phys Rev E* **101** (5) 050902 (2020)

D. Reedy, J. B. Williams, B. Gaire, A. Gatton, M. Weller, A. Menssen, T. Bauer, K. Henrichs, Ph. Burzynski, B. Berry, Z. L. Streeter, J. Sartor, I. Ben-Itzhak, T. Jahnke, R. Dörner, Th. Weber, and A. L. Landers, "Dissociation dynamics of the water dication following one-photon double ionization. II. Experiment" *Phys Rev A* **98** (5) 053430

C. W. McCurdy, T. N. Rescigno, C. S. Trevisan, R. R. Lucchese, B. Gaire, A. Menssen, M. S. Schöffler, A. Gatton, J. Neff, P. M. Stammer, J. Rist, S. Eckart, B. Berry, T. Severt, J. Sartor, A. Moradmand, T. Jahnke, A. L. Landers, J. B. Williams, I. Ben-Itzhak, R. Dörner, A. Belkacem, and Th. Weber, "Unambiguous observation of F-atom core-hole localization in CF_4 through body-frame photoelectron angular distributions" *Phys Rev A* **95** (1) 011401

A Menssen, C S Trevisan, M S Schöffler, T Jahnke, I Bocharova, F Sturm, N Gehrken, B Gaire, H Gassert, S Zeller, J Voigtsberger, A Kuhlins, F Trinter, A Gatton, J Sartor, D Reedy, C Nook, B Berry, M Zohrabi, A Kalinin, I Ben-Itzhak, A Belkacem, R Dörner, T Weber, A L Landers, T N Rescigno, C W McCurdy and J B Williams, "Molecular frame photoelectron angular distributions for core ionization of ethane, carbon tetrafluoride and 1,1-difluoroethylene" *J Phys B* **49** (5) 055203

ACKNOWLEDGEMENTS

fill in this section This work was supported by the NSF Career Award grant No. DMR-1255370, and the Simons Collaboration on Cracking the Glass Problem (No. 454939 E. Corwin)

TABLE OF CONTENTS

Chapter Page

LIST OF FIGURES

Figure Page

CHAPTER I

INTRODUCTION

When you think of solids, you generally think of crystals. You take a liquid, and let it cool down, and it falls into a nice crystal structure that is spatially optimized in some way. This is generally how most solids form and is conceptually pretty easy to understand. Glass however can be formed by cooling down a liquid too quickly to find its minimum energy configuration - it essentially just gets stuck in some non-optimal state instead. Granular materials exist in a similar way - if you've ever stacked oranges, you can arrange them quite efficiently in a FCC lattice. But if you pour them together, they will be arranged randomly. If you then squeeze the box, the oranges don't spontaneously form the FCC lattice - they are frustrated in the sense that they are all blocking each other from forming this more optimal arrangement, in the sense that you could fit more oranges in if they were arranged in a lattice. In contrast to crystalline solids, amorphous solids and granular materials are generally extremely difficult to understand from first principles. The only successful approach is in the limit of infinite spatial dimensions, termed "mean field." This seems kind of absurd, and it is - results from the mean field limit are not certain to aplpy to any finite dimensional system. Many results from the mean field however are shockingly accurate even in as low as 2 and 3 dimensions.

A phase transition is when a material undergoes a discontinuous change in some property (the "order parameter") as some other property (the "control parameter") varies. The most well known phase changes are freezing/melting and boiling/condensating, for which the temperature is the control parameter, and the density of the material can be seen to discontinuously change at critical temperatures. The order parameter is generally accepted to be the free energy - at the phase transition, melting absorbs a latent heat separate from the heat required just to heat it to the melting point. While glasses go through thermal phase transitions, granular materials do not. Granular materials are thus described as being "athermal" or "zero-temperature." If you imagine the box of oranges as described earlier, thermal fluctuations (with energy kT) will never reach the temperature required to rearrange a couple of oranges (energy mgr). Granular materials do however go through a different type of transition, called the jamming and unjamming transitions, which are similar to typical phase transitions in some ways, but different in other ways. The

control parameter for the jamming transition is the density φ, and the jamming transition happens at a particular density where properties of the system go through discontinuous changes. In particular, the pressure P goes from 0 to a finite value, and the number of force bearing contacts between granules goes from 0 to roughly the spatial dimension times the number of particles Nd. The jamming density φ_j is an exact value for any particular system, but generally has some variation between systems, and can vary based on the protocol of system generation. The jamming point can be understood as a critical point, and as the system increases in density from that point, properties such as the number of contacts in excess of ND, the pressure, and the density in excess of φ_j all scale with each other as power laws rather than having an absolute scale (e.g. exponential scalings).

Traditional approaches to analyzing thermodynamic systems rely on the assumption of ergodicity, i.e. that the thermal system explores the ensemble of all available configurations. The probability of existing in any particualar configuration is related to the energy of that configuration compared with the temperature of the system. In a zero temperature granular material, however, this is obviously impossible. Despite this, granular materials respond predictably to repeated disturbances, e.g. if you repeatedly shake a box of rocks, they will reliably settle into a configuration of roughly the same density. Thus some version of athermal statistical mechanics is clearly at work. In the 80's Sir Sam Edwards begun the first serious attempt at understanding granular materials in thermodynamic terms. The parameters compactivity and angoricity came about as analogs to temperature that relate to the density and pressure rather than temperature. While this approach has had some success, measurement of angoricity and compactivity is difficult.

The jamming transition describes the onset of rigidity. Below φ_j, a system is floppy and unable to sustain any force. Above φ_j however a system becomes rigid and can support external forces. You can run your hands through sand at the beach, but if you compress it, it will push back. This rigidity can be understood in terms of degrees of freedom and constaints - it arises when the system has at least as many constraints as degrees of freedom. A system where these are exactly equal is termed "isostatic," and a system with more constraints than degrees of freedom is termed "hyperstatic." Since each particle can move in d dimensions, a granular system has Nd degrees of freedom and the constraints to those degrees of freedom are the contacts between

particles. All of our jammed configurations that we study are hyperstatic and thus are rigid and can support external forces. When considering the force network, each contact is a degree of freedom, and requiring force balance on each particle imposes Nd constraints. Thus while the positions of particles in a hyperstatic system is overdetermined, the force network supporting this rigidity is underdetermined. There exists a degerate space of allowed force configurations, which is referred to as the "Force Network Ensemble." This was first formulated by some dutch guys in 2004, and we thought it was cool so we used it a lot.

The following three chapters are the three papers which we composed during my time as a graduate student. The first explores a method that we developed that uses the Force Network Ensemble to measure the allowed space of force configurations. This allowed us to measure the angoricity and thus the entropy of the force networks of a granular system. In the second, we use a similar approach to examine the boundaries of the allowed space of force configurations. These boundaries correspond to systems with fewer contacts than the original system. By examining which contacts are missing in those systems, we are able to predict which contacts between particles are unnecessary, and show that under decompression of a system, these contacts are in fact the ones that are lost. In the third, we closely examine the relation between the critical power laws from the jamming transition. Rather than looking at the exponents of these power laws, which are quite well known, we explore instead the prefactors to these power laws. Although prefactors are highly sensitive to finite dimensional corrections to mean field, we find that they are still well predicted by the mean field.

CHAPTER II

DIRECT MEASUREMENT OF FORCE CONFIGURATIONAL ENTROPY IN JAMMING

Abstract

Thermal fluctuations are not large enough to lead to state changes in granular materials. However, in many cases, such materials do achieve reproducible bulk properties, suggesting that they are controlled by an underlying statistical mechanics analogous to thermodynamics. While themodynamic descriptions of granular materials have been explored, they have not yet been concretely connected to their underlying statistical mechanics. We make this connection concrete by providing a first principles derivation of the multiplicity and thus the entropy of the force networks in granular packings. We directly measure the multiplicity of force networks using a protocol based on the phase space volume of allowed force configurations. Analogous to Planck's constant, we find a scale factor, h_f, that discretizes this phase space volume into a multiplicity. To determine this scale factor, we measure angoricity over a wide range of pressures using the method of overlapping histograms and find that in the absence of a fundamental quantum scale it is set solely by the system size and dimensionality. This concretely links thermodynamic approaches of angoricity with the microscopic multiplicity of the force network ensemble.

Introduction

Thermodynamics connects abstract and difficult to measure details, such as entropy, with more easily measured bulk properties, such as temperature. In granular systems, for which the thermal energy scale is irrelevantly small, similar connections have been proposed for the volume ensemble [7, 21] using compactivity as a temperature analog and also for the force network ensemble [7, 22] using angoricity. While these quantities are measurable [8, 52], they are not physically meaningful unless they 1) are shown to have temperature-like properties, such as following the zeroth law and 2) can be rigorously linked to a first principles definition of microscopic entropy [31]. Entropy itself was initially an empirical quantity until Sackur and Tetrode placed it on firm footing for the ideal gas with the discretization of phase space into quantum mechanical states [31, 64]. The length scale of the discretization depends both on properties of the system and the universal constant $\hbar$, whose value cannot be inferred from bulk

properties of the ideal gas alone. Angoricity holds promise as a temperature analog, as it has been shown to follow the zeroth law, while compactivity fails to do so [7, 23, 52]. However, before the thermodynamic approach of angoricity can be considered to be on solid ground, the nature of the entropy of jammed systems must first be understood.

When the density of an overjammed packing increases, force networks are affected in two ways: 1) force magnitudes, and thus pressure, increase, and 2) new contacts between particles form, increasing the number of contact forces in the network. Both of these changes increase the entropy of the force networks. While the effect on entropy from pressure changes is well understood [8, 32], the effect from changes in the contact network is not. To decouple these effects, we propose an extension to the Force Network Ensemble in which changes in the contact network are allowed. This leads us to identify a critical number of excess contacts, δz_c, describing the transition from a regime in which entropy is dominated by changes in pressure to one in which it is dominated by changes in the contact network.

The temperature analogue angoricity is defined as the derivative of entropy with respect to the stress tensor [22]. In isotropic systems this tensor quantity can be simplified to a scalar derivative of entropy with respect to pressure. Just as temperature of an ideal gas can be measured from the velocity distribution, angoricity can be measured from the distribution of local pressures [8]. As a derivative, angoricity provides information about the difference in entropy between two systems but not the absolute values. Previous theoretical and experimental work has identified an inverse scaling of angoricity with pressure in the near jamming limit for two-dimensional (2D) soft spheres [8, 32]. However, these studies do not systematically explore the effect of changing the contact network, which remains static in the near jamming limit. In our computational study, we explore the system by varying the spatial dimension, pressure, and number of particles over ranges much larger than would be feasible in a physical experiment.

In this Rapid Communication, we present a first principles derivation of the entropy for the force networks of granular packings. We measure this entropy up to a multiplicative constant, h_f, in the near jamming limit by directly measuring the volume of the space of allowed force configurations. Analogous to Planck's constant in the Sackur-Tetrode equation, h_f discretizes the space of force configurations into an integer number of accessible states. We then use the method of overlapping histograms to measure angoricity as a function of pressure, and compare with our

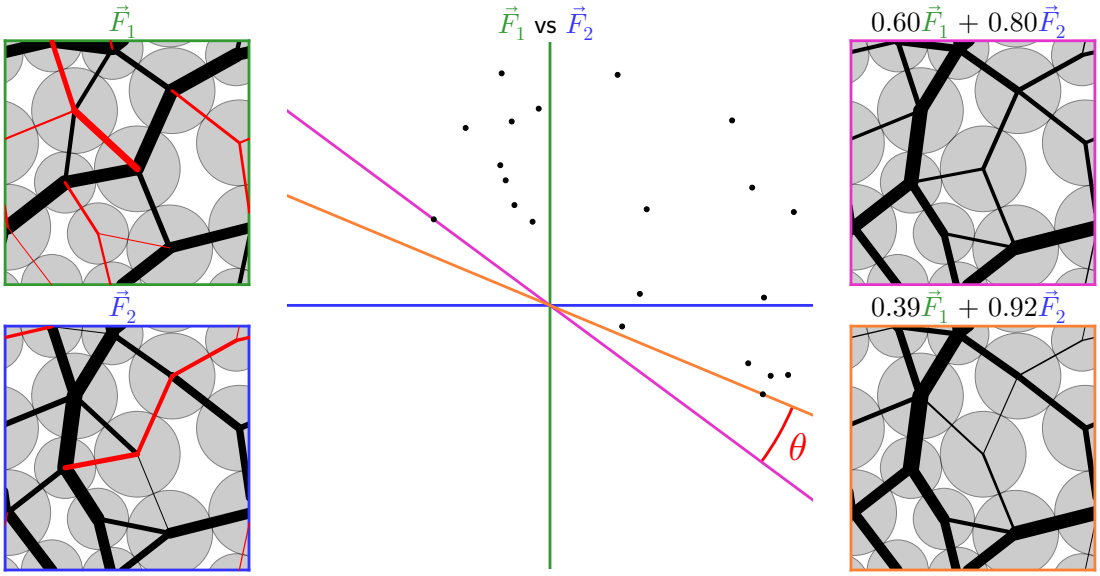

FIGURE 1. Force volume measurement for a system with one excess contact. Left, the two independent states of self stress, F_1 and F_2. Black lines between particles represent positive (compressive) forces, red lines represent negative (tensile) forces. Center, a scatter plot of F_1 vs F_2 for each pair of particles. Linear combinations of F_1 and F_2 are represented graphically by drawing a sloped line through the origin and measuring the distance to each point. Any sloped line for which all of the points fall into the same half-space corresponds to a positive definite linear combination. The set of lines which allow for such solutions is the force space volume, indicated by the angle θ. Note that in a system with ΔZ excess contacts, this volume is a ΔZ dimensional quantity. Right, the two extremal positive-definite linear combinations at the edge of this region are shown. Each has one force brought to precisely zero.

force volume measure to solve for h_f. This concretely connects the bulk nature of angoricity with the microscopic multiplicity of the force network ensemble.

Computational methods

We use pyCudaPacking [13], a GPU-based simulation engine, to generate energy minimized soft sphere packings at specified pressures in periodic boundary conditions. We do so for number of particles, N, spanning from 256 to 4096, and dimension, d, from 2 to 5. The particles are monodispersed, except in 2D in which we use equal numbers of bidispersed particles at a size ratio of 1.4:1 to prevent crystallization. Particles interact through a harmonic contact potential as defined in [13], and the system's energy is minimized using the FIRE minimization algorithm [9].

Starting with random initial positions, we minimize energy and then adjust overall density by uniformly scaling particle radii to achieve a pressure P of 10^{-2} in natural units, as defined in

[45]. This pressure is chosen to prevent crystallization artifacts from high density packings. From there, we iteratively adjust the density both up and down to achieve specific values of pressure. We do this efficiently by exploiting the known linear scaling of pressure with density above jamming for a harmonic potential [30]. For each targeted pressure, we ensure that the actual pressure is accurate to a factor of 10^{-5}. We sample 100 logarithmically spaced steps per decade of pressure to ensure sufficient overlap between the distributions of local pressure for neighboring systems, as is needed for the method of overlapping histograms.

Rigidity

To understand the behavior of packings close to the jamming transition we examine the geometric mechanisms necessary for rigidity by constructing an unstressed spring network with the geometry of the packing. The rigidity matrix [14, 24, 25], $\mathcal{R}$, describes this spring network by encoding the normalized contact force vectors from the packing, n_{ij}, between pairs of particles i and j as

$$\mathcal{R}^{k\alpha}_{\langle ij \rangle} = (\delta_{jk} - \delta_{ik}) n^{\alpha}_{ij}, \tag{2.1}$$

where k indexes contacts and α indexes spatial dimensions. For a system with N_{stable} stable particles and N_{contact} contacts, this will be an N_{contact} by $N_{\text{stable}}d$ matrix. The singular value decomposition of this matrix yields two sets of singular vectors, analogous to eigenvectors for a square matrix. The right singular vectors describe the normal modes of position displacements, and the left singular vectors describe the normal modes of force displacements. The left singular vectors corresponding to zero eigenvalues represent mechanically stable force configurations, termed states of self stress. These vectors need not be positive definite, and therefore are not necessarily valid force configurations for the underlying packing.

The magnitude of each contact force can be considered as a degree of freedom while the requirement for mechanical stability introduces d constraints for each particle. Balancing these constraints requires a minimum number of contacts to ensure stability, which in systems with periodic boundary conditions is given by [18, 28]

$$N^{\text{min}}_{\text{contact}} = d(N_{\text{stable}} - 1) + 1. \tag{2.2}$$

A system with this minimum number of contacts has exactly one state of self stress, and each additional contact formed imparts an additional independent state of self stress. Thus, we define the number of excess contacts, ΔZ as

$$\Delta Z = N_{\text{contact}} - N_{\text{contact}}^{\min}, \tag{2.3}$$

making the number of independent states of self stress $\Delta Z + 1$. We define the number of excess contacts per particle,

$$\delta z = 2\Delta Z/N, \tag{2.4}$$

where the 2 reflects that each excess contact is shared between two particles. These independent states of self stress form a basis for the $\Delta Z + 1$ dimensional space of all mechanically stable force configurations of the spring network. However, imposing a normalization condition restricts this to a ΔZ dimensional subspace.

Force Volume

The force network ensemble samples all valid force networks in the spring representation of a packing with equal probability [61, 65, 66]. To determine the force volume, we calculate the normalized independent states of self stress where F_μ^q is the contact force on contact q in the state of self stress μ. The set of all possible repulsive contact forces is defined by linear combinations that satisfy

$$\sum_\mu \lambda_\mu F_\mu^q \geq 0 \tag{2.5}$$

for all contacts q, where $\{\lambda_\mu\}$ are coefficients subject to the normalization condition $\sum_\mu \lambda_\mu^2 = 1$. We define the force volume V_f to be the volume of the space of λ_μ coefficients that satisfy this rule as illustrated in Fig. 1.

We measure this force volume with the following protocol:

1. Recast F_μ^q into a set, $\{\vec{C}^q\}$, of N_{contacts} vectors containing the value of the force on contact q in each of the $\Delta Z + 1$ states of self stress.

2. Planes which pass through the origin and place all of the $\{\vec{C}^q\}$ into a single half-space satisfy inequality (2.5). We compute the extremal values of such planes as the facets of the convex hull [4] of $\{\vec{C}^q, \vec{0}\}$. The normal vector to each facet is the $\{\lambda_\mu\}$ which defines a vertex of the allowed space of coefficients and corresponds to a linear combination of the independent states of self stress in which exactly ΔZ forces are precisely 0.

3. To respect the normalization requirement we calculate V_f as the ΔZ dimensional solid angle subtended by the volume defined by these vertices in coefficient space.

We convert this volume into a pure number of configurations by discretizing it into hypercubes of side length h_f, named to emphasize the parallelism with Planck's constant h used in the enumeration of phase space states in the Sackur-Tetrode equation. Because the pressure sets the scale of the average force, we then multiply this enumeration by the pressure, as has been shown in previous theoretical and experimental work [8, 32, 37]. Putting these considerations together, we arrive at an ansatz relating the microscopic force volume to the multiplicity, and thus the entropy:

$$\Omega = P\frac{V_f}{(h_f)^{\Delta Z}} \qquad \Longrightarrow \qquad S = \ln P + \ln V_f - \Delta Z \ln h_f. \tag{2.6}$$

Although pressure and number of excess contacts both appear in the entropy, they are not independent variables but related in the thermodynamic limit by [30, 45]

$$\Delta Z = B(d) N \sqrt{P}. \tag{2.7}$$

where B is some function of dimension only. We find values of B of approximately 2.1, 6.0, 12.5, and 23 in dimensions two, three, four, and five. These values are roughly consistent with previous studies for two and three dimensional spheres [28, 45].

Angoricity [22], α, is derived as:

$$\alpha \equiv \frac{\partial S}{\partial P} = \frac{1}{P} + \frac{\partial}{\partial P}\ln V_f - \frac{1}{2}\frac{BN}{\sqrt{P}}\ln h_f. \tag{2.8}$$

First, we measure the volume of force space V_f and explore how it scales with the number of excess contacts. Second, we measure bulk angoricity to confirm our prediction in Eq. (2.8) and measure the microscopic constant h_f.

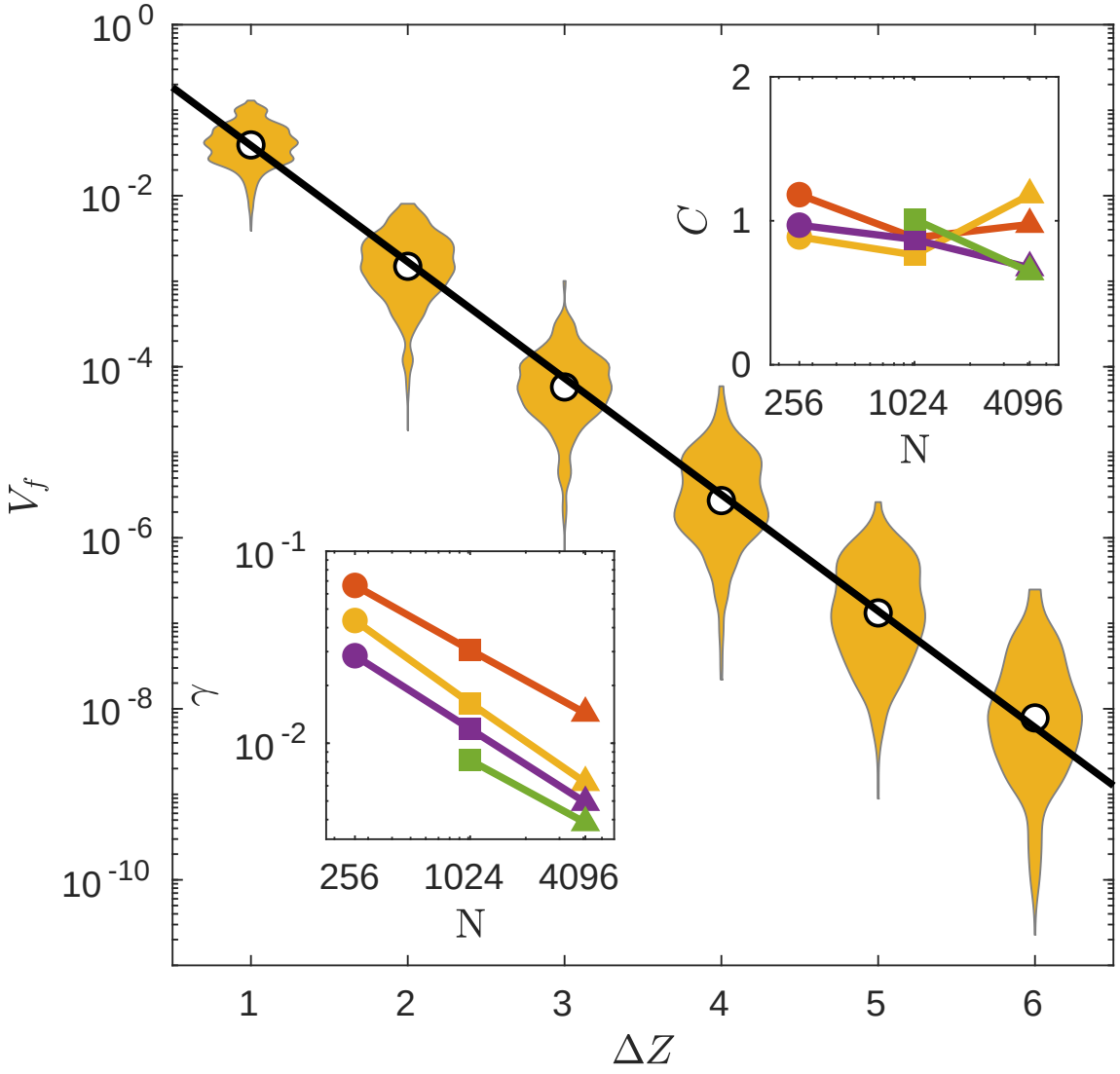

FIGURE 2. Representative exponential scaling of the force volume, V_f, with number of excess contacts, ΔZ, for $N = 1024$, $d = 3$. The median of the distribution for each ΔZ is shown as a white circle, surrounded by the full distribution in yellow. The black line shows the exponential fitting form, with exponential base γ. Inset bottom left, γ for each N and d. Inset top right, the scale, C of the exponential. Inset data is presented for $d = 2$ (red), 3 (yellow), 4 (purple), and 5 (green), and $N = 256$ (circles), 1024 (squares), and 4096 (triangles).

Results

As shown in Fig. 2, the measured force volume scales exponentially with the number of excess contacts:

$$V_f \;=\; C\gamma^{\Delta Z}. \tag{2.9}$$

We find C to be well approximated by 1, as shown in the top inset. The lower inset shows that γ decreases with increasing N and d.

We can simplify the expression for angoricity by combining the preceding three equations to find

$$\alpha = \frac{1}{P} + \frac{1}{\sqrt{P_c P}} \tag{2.10}$$

where the crossover pressure between the two power laws is

$$P_c = \left[\frac{BN}{2}\ln\left(\frac{\gamma}{h_f}\right)\right]^{-2}. \tag{2.11}$$

We use the method of overlapping histograms of local pressures [5, 8, 40] to measure angoricity and determine the value of P_c and therefore h_f. For each system, we measure the local pressure for many random samples of a particle with its $m = 50$ nearest neighbors. The choice of m controls the sharpness of the local pressure distribution and so induces a trivial prefactor A, shown in the inset to Fig. 3 to be proportional to dm. We then compute the angoricity by comparing these local pressure distributions as in Ref [8]. We fit the angoricity curve to the power law in Eq. (2.10) with prefactor A and an additive offset. As shown in Fig. 3, all data collapse onto Eq. (2.10). We extract the crossover pressures, P_c, shown in the upper inset of figure 3, and find that they are insensitive to N, but decrease with increasing d.

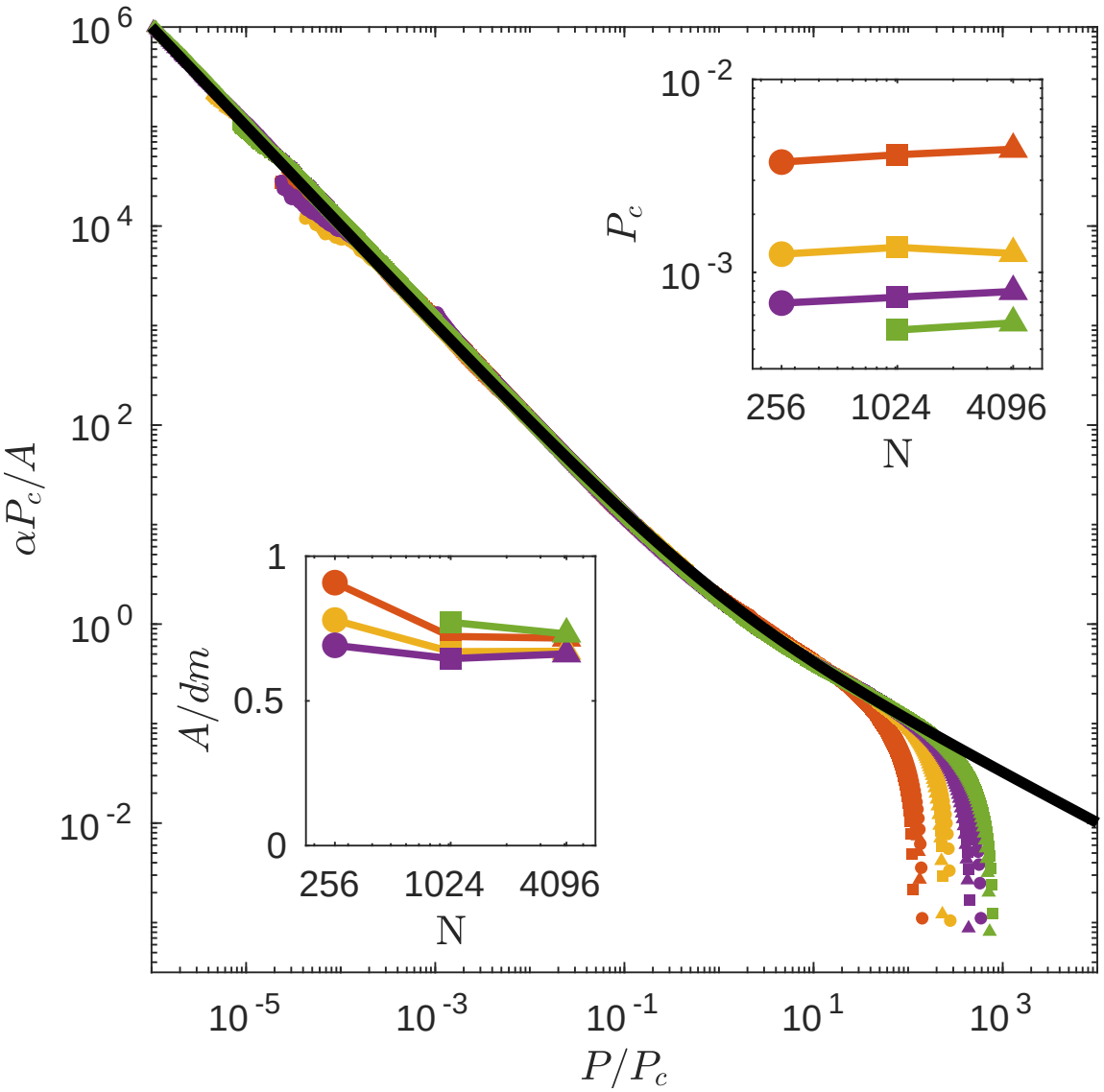

FIGURE 3. Scaled angoricity, $\alpha P_c/A$, for all N and d, collapses onto equation 2.8 (black line) when plotted against scaled pressure, P/P_c, until high pressure deviations caused by second nearest neighbor interactions. Inset top right, the crossover pressure P_c. Inset bottom left, A/dm is approximately 0.7. Colors denote dimension from 2-5 and symbol denotes number of particles as in figure 2.

Discussion

From Eq. (2.11) and our measured values of γ and P_c we compute h_f, shown in the inset to Fig. 4. A complete expression for entropy can now be written as

$$S = \ln P + \Delta Z \ln\left(\frac{\gamma}{h_f}\right). \tag{2.12}$$

This can be recast into a natural form using equations (2.7) and (2.10) by expressing the ratio of γ and h_f as a critical number of excess contacts per particle,

$$\delta z_c = 2B\sqrt{P_c} = \frac{2}{N \ln\left(\frac{\gamma}{h_f}\right)} \tag{2.13}$$

$$S = \ln P + \frac{\delta z}{\delta z_c}. \tag{2.14}$$

Thus, the entropy is dependent on two intensive thermodynamic variables, P and δz, and a constant δz_c for each dimension. While h_f is observed to decrease with N and expected to vanish in the thermodynamic limit, we find δz_c to be intensive with system size, as shown in Fig. 4.

The first term in Eq. (2.14) describes the entropy increasing from the absolute pressure scale, whereas the second describes the entropy increasing from the number of contacts increasing. Sufficiently close to jamming the first term will dominate as there will be few changes in the contact network even as the pressure changes dramatically. Further from jamming the second term will dominate, reflecting the primacy of changes in the contact network. Note that while this equation may be rewritten as a function of pressure using Eq. (2.7), for any particular finite packing the integer number of excess contacts is required to calculate the entropy precisely.

Conclusion

We have demonstrated that the force network ensemble framework can be used to directly compute the multiplicity of the force configurations in packings close to the critical jamming point. We have presented an ansatz linking the volume of the force configurational space associated with a packing to the entropy of the packing. This entropy can be expressed as a function of pressure and is independently confirmed by measurements of the angoricity over approximately seven orders of magnitude of pressure. We have combined these two approaches of measuring entropy in order to extract the fundamental scales governing the discretization of phase space that allows for enumeration. We discover a crossover value for the excess contacts per particle, δz_c, below which the entropy is governed primarily by changes in pressure at fixed contact network and above which the entropy is governed primarily by the creation of new contact forces.

This work places angoricity on a firm footing as a thermodynamic quantity that controls the behavior of overjammed systems. By tracing this entropy all the way down to an enumeration of states we discover that, perhaps unsurprisingly, Planck's constant does not set the fundamental scale of discretization h_f. In a purely classical model such as this, the discretization can only depend on the finite size effects of the system which are determined by N and d. Thus, in the thermodynamic limit, while h_f vanishes, the behavoir of the system is controlled by δz_c and thus P_c which do obtain fixed values. This full expression for entropy provides the first concrete linking of the microscopic force network ensemble to the thermodynamic description of granular materials and offers a complete description for the thermodynamics of the force networks in overjammed systems.

Acknowledgments

We thank Bulbul Chakraborty, Karen Daniels, Sean Ridout, and Brian Tighe for useful discussions. This work benefited from access to the University of Oregon high performance computer, Talapas. This work was supported by National Science Foundation (NSF) Career Award DMR-1255370 and the Simons Foundation Grant No. 454939.

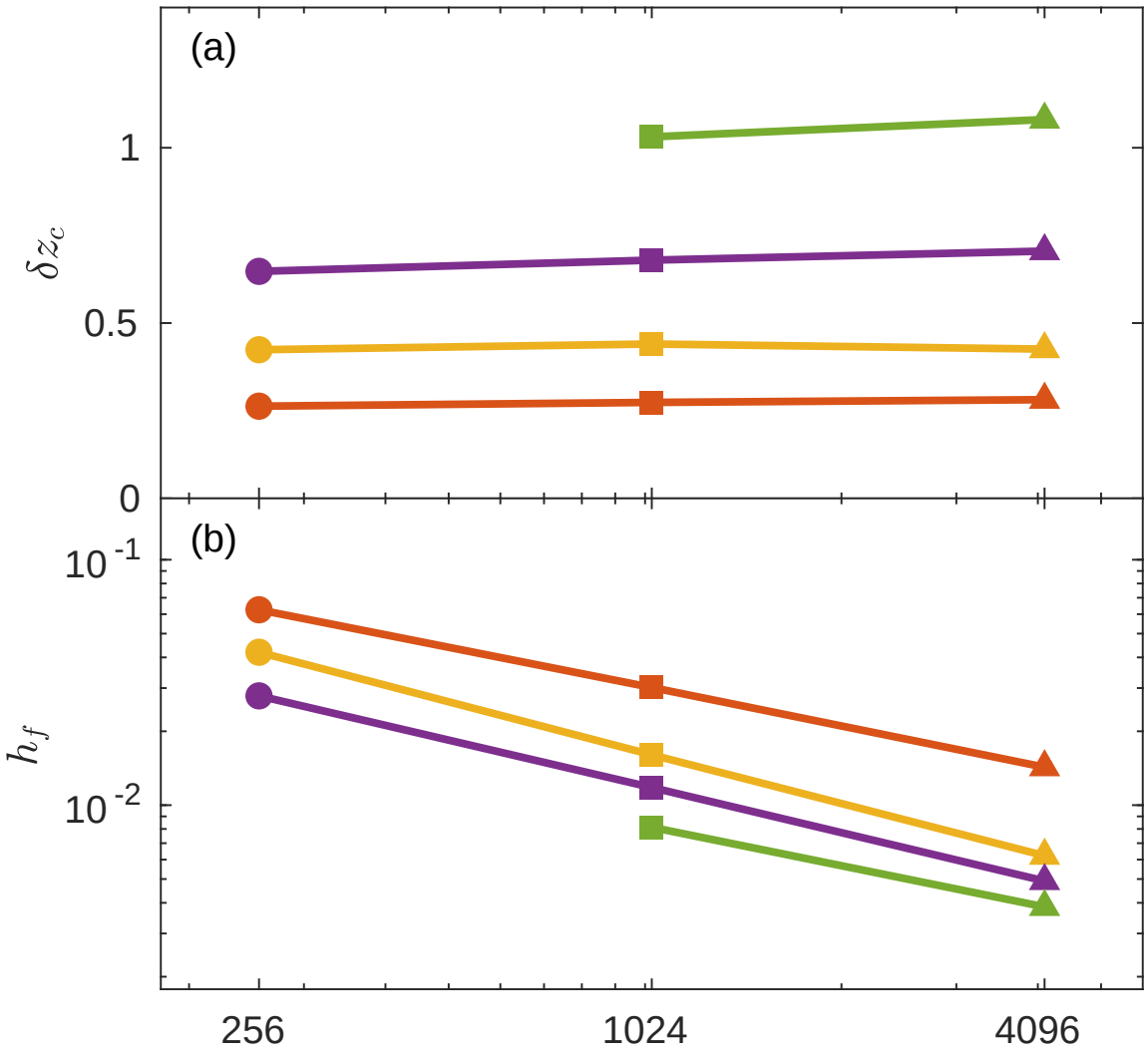

FIGURE 4. Upper, scaling of δz_c with N and d. Lower, scaling of h_f, with N and d, calculated from P_c by inverting equation 2.11. Colors denote dimension from 2-5 and symbol denotes number of particles as in figure 2.

CHAPTER III

PREDICTING DEFECTS IN SOFT SPHERE PACKINGS NEAR JAMMING USING THE FORCE NETWORK ENSEMBLE

Abstract

Amorphous systems of soft particles above jamming have more contacts than are needed to achieve mechanical equilibrium. The force network of a granular system with a fixed contact network is thus underdetermined and can be characterized as a random instantiation within the space of the force network ensemble. In this work, we show that defect contacts which are not necessary for stability of the system can be uniquely identified by examining the boundaries of this space of allowed force networks. We further show that in the near jamming limit, this identification is nearly always correct and the defect contacts are broken under decompression of the system.

Introduction

From crafting swords and arrowheads in antiquity to perusing katanas at the mall today, choosing the available materials with highest strength has always been of critical concern. It is the weak points, and modes of failure, that determine the strength of a material. In polycrystalline materials these weak points arise from defects in the crystal structure [63]. Early approaches to amorphous systems attempted to model them as highly defective crystalline systems, but such models fail to capture emergent phenomena [29]. Amorphous systems thus must be treated in their own right, consequently there exists no obvious definition of a defect. However, "soft spots" can be found which are locations in which rearrangements are more likely to occur under shear. These were first explored via analysis of the low-frequncy quasilocalized vibrational modes [38] and have been more recently identified by using machine learning analysis on the local structure [16, 17, 20, 53–55, 58, 59, 68]. While this has been highly effective at identifying sites of rearrangements under shear, it has not been applied to systems under decompression, another common failure mode of materials. More importantly, while softness is correlated with structural quantities such as local potential energy and coordination number, these structural properties are not good predictors of rearrangements on their own. Thus softness, while useful as a heuristic,

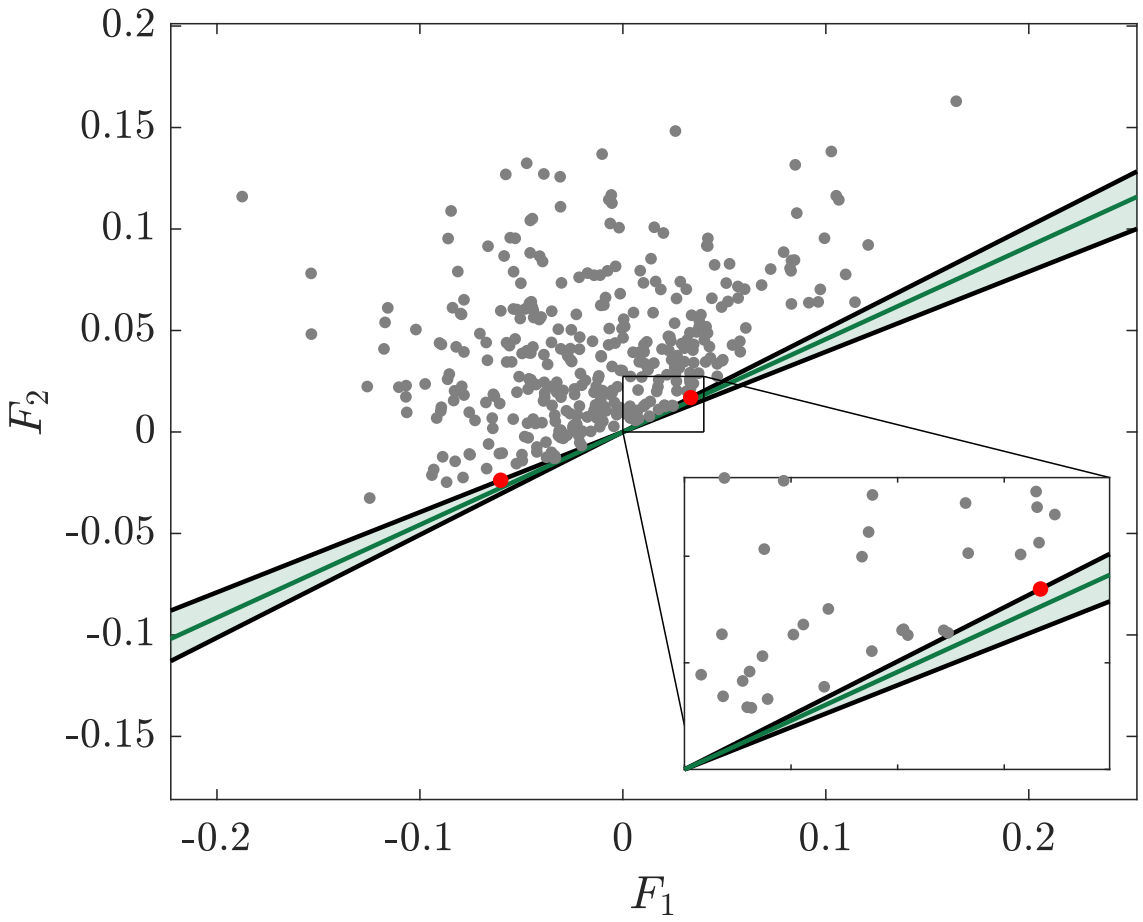

FIGURE 5. Scatter plot of the loads on each contact in the two states of self stress F_1 and F_2 for a typical system ($N = 128$) at 2SSS. Black lines represent the two linear combinations of force eigenvectors at the boundary of the allowed region of force space, shaded green. The two contacts which define these boundaries are shown in red. Green line shows linear combination that reconstructs the measured physical forces. Inset shows a region near the origin in greater detail. For a more pedagogical explanation see figure 1 in [56].

lacks analytic clarity. Additionally, while softness is an excellent predictor of instabilities, it does not predict stable contact network changes (i.e. contact changes which do not result in rearrangements), which comprise the majority of contact network changes [41, 67]. In this work we demonstrate a method for identifying defective contacts under decompression asymptotically close to the jamming/unjamming transition. We use the geometry of the force network ensemble to show that in the near-jamming limit there exists only a small and precisely identifiable number of contacts at which any contact network change can occur.

Background

To achieve mechanical stability, any system must have at least as many constraints as degrees of freedom. In a granular system, these constraints are borne by the contacts, and for a d dimensional system of frictionless spheres, the minimum number of contacts $N_c^* \sim Nd$ [39]. Any system that posseses more than this minimum number of contacts will have a resultant indeterminacy in its force networks as there must exist multiple linearly independent solutions for force balance. Near jamming, the overlaps (or deformations) between particles are much smaller than the interparticle distances. Due to this separation of scales, the forces in a system can be decoupled from the particle positions, and therefore can be considered to be a random instantiation within the space of the force indeterminancy [56, 61, 65, 66]. This is the motivation for the force network ensemble (FNE), which samples all valid force networks in the spring representation of a packing with equal probability.

The rigidity matrix, $\mathcal{R}$, represents a granular system as an unstressed spring network by encoding the normalized contact force vectors $\hat{n}_{ij}$ between pairs of particles i and j as

$$\mathcal{R}^{k\gamma}_{\langle ij \rangle} = \left(\delta^k_j - \delta^k_i\right) \hat{n}^\gamma_{ij}, \tag{3.1}$$

where k indexes particles, γ indexes spatial dimensions, and δ is the Kronecker delta [14, 24, 25, 56]. In periodic boundary conditions the minimum number of contacts required for stability for N particles in dimension d is [28]

$$N_c^* = Nd - d + 1, \tag{3.2}$$

and a system with exactly N_c^* contacts will have one stable force network configuration. For each additional contact in excess of N_c^* the associated unstressed spring network will have an additional linearly independent mechanically stable force network. These linearly independent force networks are referred to as the "states of self stress" or SSS of the system. These can be easily computed as they are the left singular vectors of $\mathcal{R}$ associated with the zero singular values of $\mathcal{R}$, i.e. the vectors F_i such that $F_i\mathcal{R} = \vec{0}$. While these SSS in general contain compressional as well as tensional forces, physical packings of frictionless spheres are constrained to compressional

forces. Thus we consider the FNE to be the set of linear combinations of the SSS which are positive semidefinite.

In previous work, we demonstrated that by considering the geometric nature of the SSS of a system, one can calculate the volume of the positive semidefinite linear combinations and from that the entropy of the force networks [56]. Further contemplation of this geometry has led us to examine the boundaries of this volume, which correspond to sets of contacts which are extraneous to the mechanical stability of the system. In particular, we focus on systems with exactly 2 states of self stress (2SSS), which are thus geometrically confined to have exactly two such boundaries. Each boundary corresponds to a set of contacts (typically each containing exactly one contact) which are unnecessary for mechanical stability of the packing. The breaking of this unnecessary contact results in a packing with just a single SSS (1SSS). In this work, we show that (i) between rearrangements, the force network ensemble of a system is stable under decompression, and (ii) that these boundaries of the volume of allowed force space identify the contacts that may be broken under decompression.

Computational Methods

We use pyCudaPacking [13], a GPU-based simulation engine, to generate monodispersed three dimensional harmonic soft sphere packings in periodic boundary conditions. We minimize the packings using the FIRE minimization algorithm [9] using quad precision floating point numbers in order to achieve sufficient resolution on the contact network near the jamming point. Using the same methods as in Refs. [42, 57], we start with randomly distributed initial positions at a packing fraction φ far above jamming and apply a search algorithm to create systems approximately logarithmically spaced in excess packing fraction, $\Delta\varphi$. We generate systems finely spaced in $\Delta\varphi$ (100 steps/decade) so that we may probe the dynamics of the transition from 2SSS to 1SSS. We continue this process until the system has exactly one state of self stress. We generate datasets of 500 systems at $N = 128, 1024$ and 100 systems at $N = 8192$. We measure the pressure P from the trace of the stress tensor as in Ref. [45] and denote the pressure at which the system transitions from 2SSS to 1SSS as P^*.

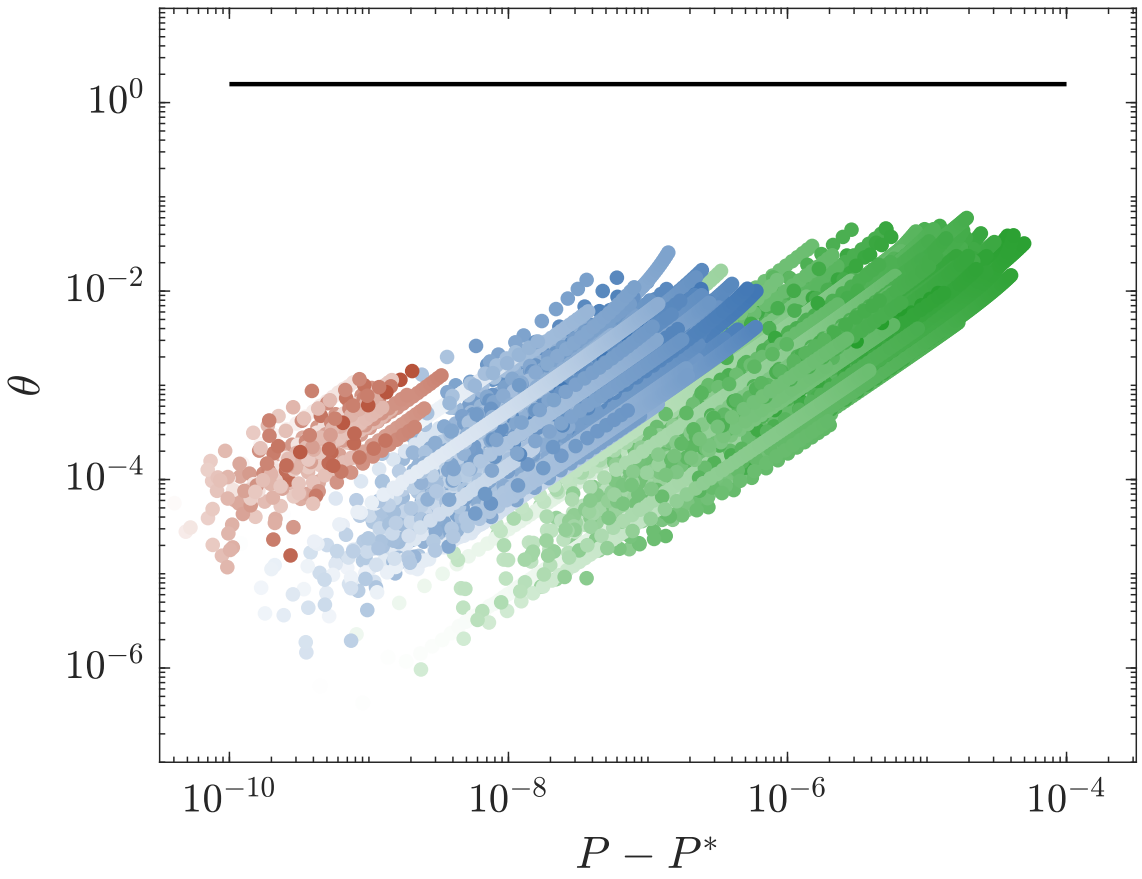

FIGURE 6. Angle θ between the force spaces of a system at a pressure P and P^*. Perpendicular force spaces would have $\theta = \pi/2$, shown as a black line. Data shown for N=128 (green), 1024 (blue), and 8192 (red), with opacity proportional to P.

Results

The force network ensemble is the set of linear combinations of these SSS for which all forces are positive semi-definite. This defines a region in force space, the boundaries of which are the linear combinations of the SSS that bring the load on a contact or set of contacts to zero. In a system with 2SSS, one can exploit the orthogonality of the SSS to choose the linear combination that yields zero force on any given contact. The imposition of this constraint necessarily reduces the number of SSS by one, and within the context of the force network ensemble is equivalent to breaking a contact. However, with most contacts, this will result in negative forces (i.e. tensile loads) on some of the contacts unless the contact chosen is on the boundary of the allowed volume of force space. We demonstrate this geometrically in figure 5.

As a system decompresses, the geometry of the contact network changes. This is reflected in the rigidity matrix and thus results in changes in the null space of the loads. Since our systems are at 2SSS, this null space is always a two-dimensional plane within the N_c dimensional space of allowed loads on bonds. We characterize how this plane evolves by computing its angle θ relative to its final configuration at $P = P^*$. We define the angle θ between 2SSS force spaces $\mathcal{F}$ and $\mathcal{G}$ (with basis vectors $\hat{F}_i$ and $\hat{G}_i$) as [33]:

$$\cos(\theta) = \frac{|\wedge^2 g(\mathcal{F},\mathcal{G})|}{\sqrt{\wedge^2 g(\mathcal{F},\mathcal{F}) \wedge^2 g(\mathcal{G},\mathcal{G})}} \tag{3.3}$$

where

$$(\wedge^2 g)(\mathcal{F},\mathcal{G}) = \det \begin{pmatrix} \hat{F}_1 \cdot \hat{G}_1 & \hat{F}_1 \cdot \hat{G}_2 \\ \hat{F}_2 \cdot \hat{G}_1 & \hat{F}_2 \cdot \hat{G}_2 \end{pmatrix}. \tag{3.4}$$

While uncorrelated 2 dimensional planes drawn through the N_c dimensional force space are nearly perpendicular (i.e. $\theta \sim \frac{\pi}{2}$), we show in figure 6 that the force space volumes of our systems are always nearly aligned, even over wide ranges of pressure. This shows that the force network ensemble of a packing is stable under decompression, at least between rearrangements. Thus, it should be possible to use the force network ensemble to predict the evolution of the physical forces as the pressure is varied.

In a system at 2SSS, the space of normalized linear combinations of the SSS is a one dimensional space of rotations, as any stable force configuration f can be described by a mixing angle α such that $f = \sin(\alpha)F_1 + \cos(\alpha)F_2$, where F_1 and F_2 are the linearly independent SSS. While the physical forces in the packing are instead calculated from the overlaps, they represent a stable force network and as such we are always able to express them with a mixing angle in this way, up to machine precision and an overall scale factor. In the intervals between contact changes, we may thus consider the physical forces in the packing as flowing within this space of SSS, which is only gently changing as shown in figure 6. In figure 7(a), we show the mixing angles that describe the position within this space for the physical forces of a 2SSS system as it decompresses towards $P = P^*$. By following these mixing angles as a system decompresses, we see how the physical forces in the system approach and reach one of the 1SSS states on the boundaries of the 2SSS space. As an example, we can follow the upper red curve in figure 7(a) down in pressure

towards the contact break, and we see that this system has a kink around $(P - P^*)/P^* \sim 1.3$. This arises from the exchange of the contact that originally formed the boundary of the allowed force space for another, which can be seen graphically in figure 7(b). Thus a prediction made with the boundary contact above that pressure will fail. The interchange in this manner of boundary contacts with other contacts that were intitially near the boundary is relatively unusual and is the sole failure mode of our prediction.

In a 2SSS system, there are always exactly two boundaries on the edge of the force space which correspond to two sets of "breakable contacts." Each of these sets of contacts usually contains just one contact, but sometimes breaking a contact will form a rattler particle, all of whose contacts will thus be in the set of breakable contacts. In figure 8, we show the probability that one of these sets of "breakable contacts" is in fact broken under decompression from 2SSS to 1SSS. We find that the contacts predicted by the FNE are strongly predictive (greater than 80%) over the full range of pressures for which the system has 2SSS. This is in sharp contrast to the naïve prediction from affine response, that the smallest contact will break. Affine response is predictive very close to the contact breaking event, but falls to zero at higher pressures.

We examined the real space correlations between pairs of breakable contacts and found no correlation in position or angle subtended between contact vectors. However, we find that breakable contacts are more likely to occur between particles with higher than average contact number ($z \sim 6.4$). Such particles are thus more likely to have a contact that is unnecessary for system stability. This stands in contrast to the soft spot literature, in which particles with fewer contacts are identified as more likely to rearrange [38, 53–55]. This difference arises because soft spots exclusively identify instabilities, but the FNE also predicts the more numerous stable contact changes involving more highly coordinated particles.

At 2SSS, the two "breakable contacts" are excellent predictors of contact breaking events. At increased pressure, the number of contacts and thus SSS increase. In figure 9, we examine the relationship between the number of predicted breakable contacts, N_{bc} and the number of states of self stress, N_{SSS}. We examine the scaling of N_{bc} as a function of the dimensionality of the normalized SSS, $d_{SSS} = N_{SSS} - 1$. At 2SSS, the breakable contacts exist at the endpoints of a line which represents the space of allowed mixing angles. This typically results in two breakable contacts, one at each endpoint, but may instead result in $N_{bc} \geq 5$ by creating a rattler at one

endpoint (i.e. four or more contacts lost at that endpoint). We rarely find $N_{bc} = 3, 4$ which can only arise from degeneracies or numerical instabilities in the 1SSS force network. At 3SSS, the boundaries of the allowed force space are the edges of a polygon, and at higher SSS the facets of a polytope. These polytopes must have at least d_{SSS} boundaries, but may have arbitrarily many and thus arbitrarily many breakable contacts. We characterize the distribution of number of breakable contacts at each SSS by their mean, and find the means to be well fit by a power-law.

We conjecture that even at higher than 2SSS, the FNE may be used to predict contact breaking events. It has recently been shown that 86% of contact breaking events are reversible network events rather than rearrangements [41, 67]. We would thus expect that these reversible contact breaking events are well described by the FNE, and as such one could use our methods to predict the possible final 1SSS systems from a system with several contacts over 2SSS, with a success probability that scales as $P \sim 0.86^{d_{SSS}}$. We note however that while the physical forces of our packings were found precisely in the force network ensemble, this may fail at significantly higher pressures, because the force network ensemble is calculated from the unstressed spring network representation of a packing, whereas there exists a prestress on the physical forces.

Conclusions

We have shown that the force network ensemble of jammed systems remains approximately static between contact change events, and as such may be used to identify defective contacts. We have further shown that for 2SSS systems, these identified defective contacts are highly likely to break under decompression. While in spirit these defects can be thought of as analogous to soft spots, we emphasize two key differences here: (1) Soft spots identify locations of instabilities, while the force network ensemble identifies locations of both instabilities and stable contact network changes, and (2) While soft spots may be identified using just local information, the FNE approach by definition invokes global information. One might wish to use local information to find these defects, and there exists local structure to the force networks when the system is far from jamming [62]. However, at the jamming point the system becomes marginal, and as such any change in the contact network impacts the whole force network. For this reason we believe that it would not be possible to identify these defective contacts near jamming without global information.

By restricting our study to 2SSS systems under decompression, we have explored only a limiting case of the space of the force network ensemble. We hope however that this serves as a gateway for future work, especially in exploring the force network landscape for systems with a greater number of SSS, where many more defects are predicted. One could also apply a modified version of these methods to identify force network defects in systems under shear. Our protocol identifies both stable contact changes and those that lead to instabilities. One further interesting remaining question is whether these can be differentiated from each other via the force network ensemble, giving a more complete picture of the defects within the system.

Acknowledgements

We thank Varda Hagh, Sean Ridout, Brian Tighe, Rafael Díaz Hernández Rojas, and Peter Morse for valuable discussion and feedback. This work is supported by the Simons Collaboration on Cracking the Glass Problem via award No. 454939.

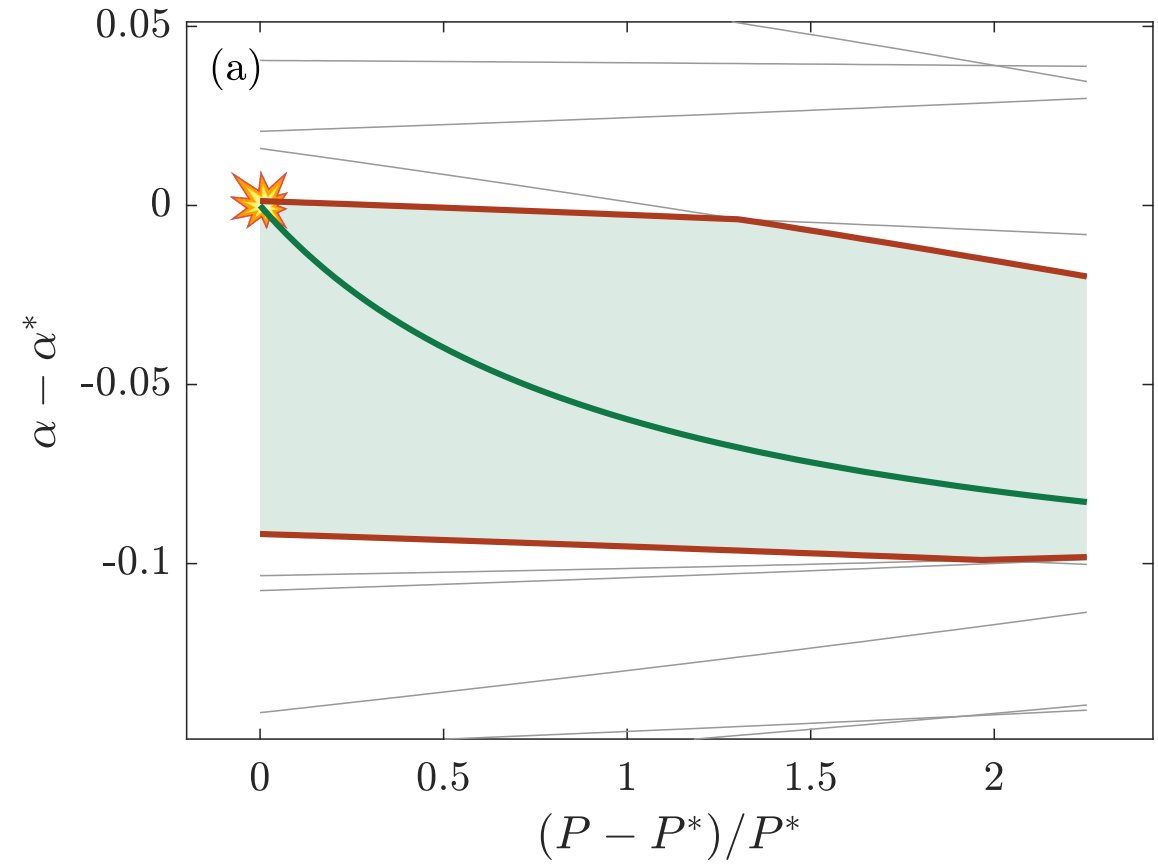

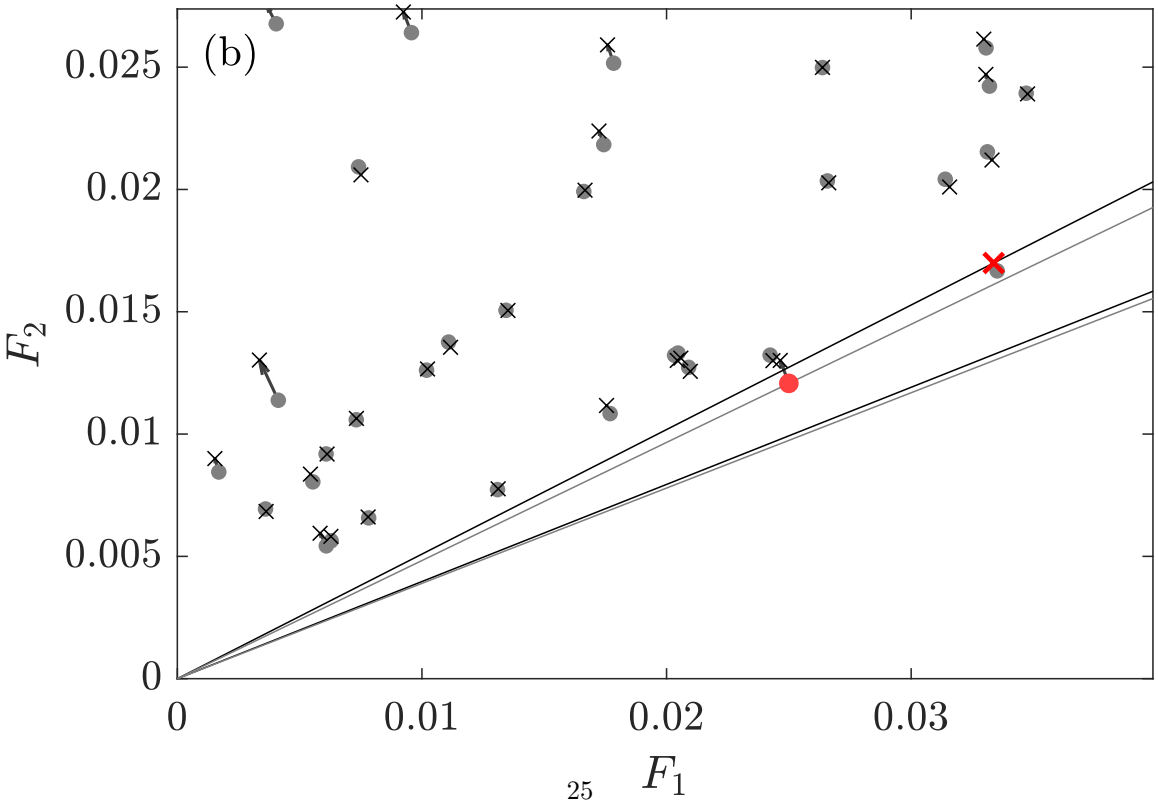

FIGURE 7. a) Evolution of mixing angle representation of the force space under decompression for the system in figure 5 over the range of pressures for which the system is at 2SSS. Position in force space is shown as mixing angles $\alpha - \alpha^*$ where α^* is the mixing angle of the system at the contact breaking event. Green shaded region shows all mixing angles for positive-definite

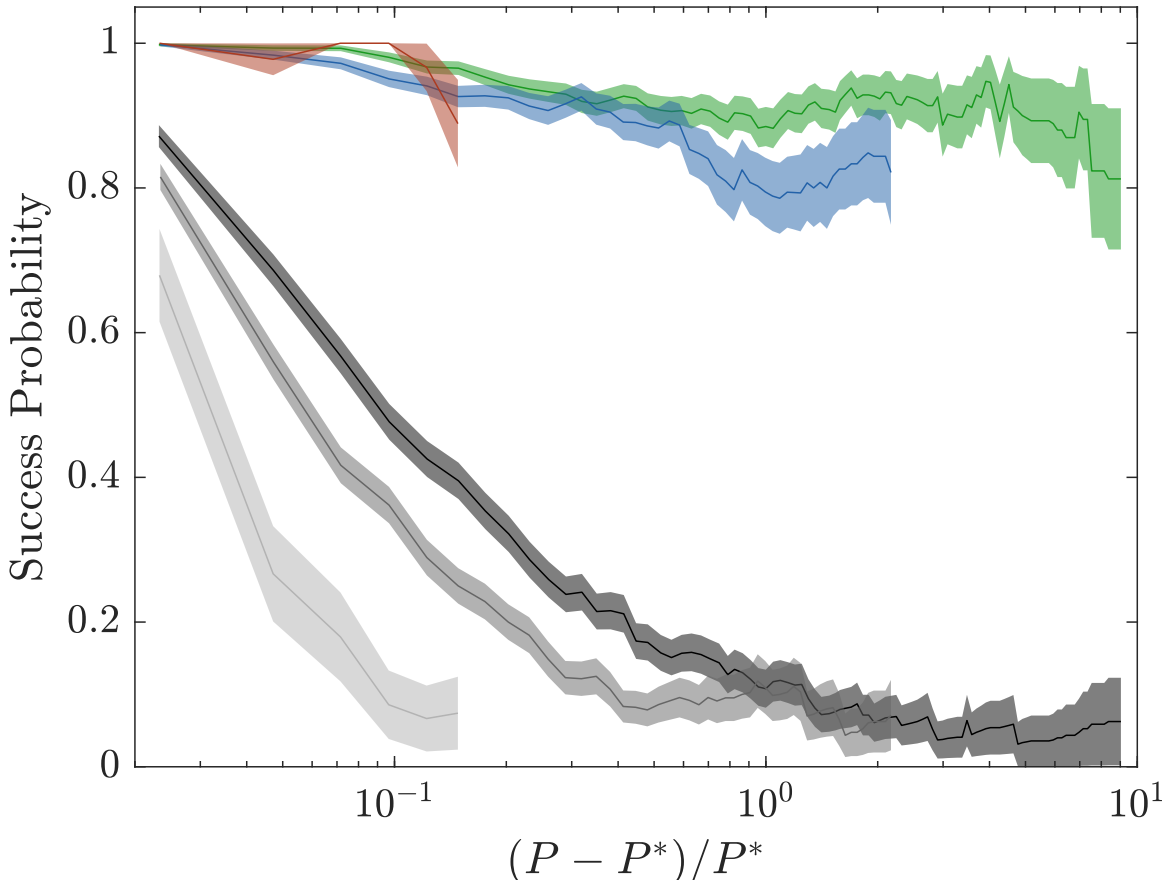

FIGURE 8. Probability of predicting contact breaking by FNE versus scaled pressure, for systems decompressing from 2SSS to 1SSS. As in fig. 6, N=128 (green), 1024 (blue), 8192 (red). Probability of smallest force in the system breaking is shown for $N = 128$ (dark grey), 1024 (medium grey), 8192 (light grey).

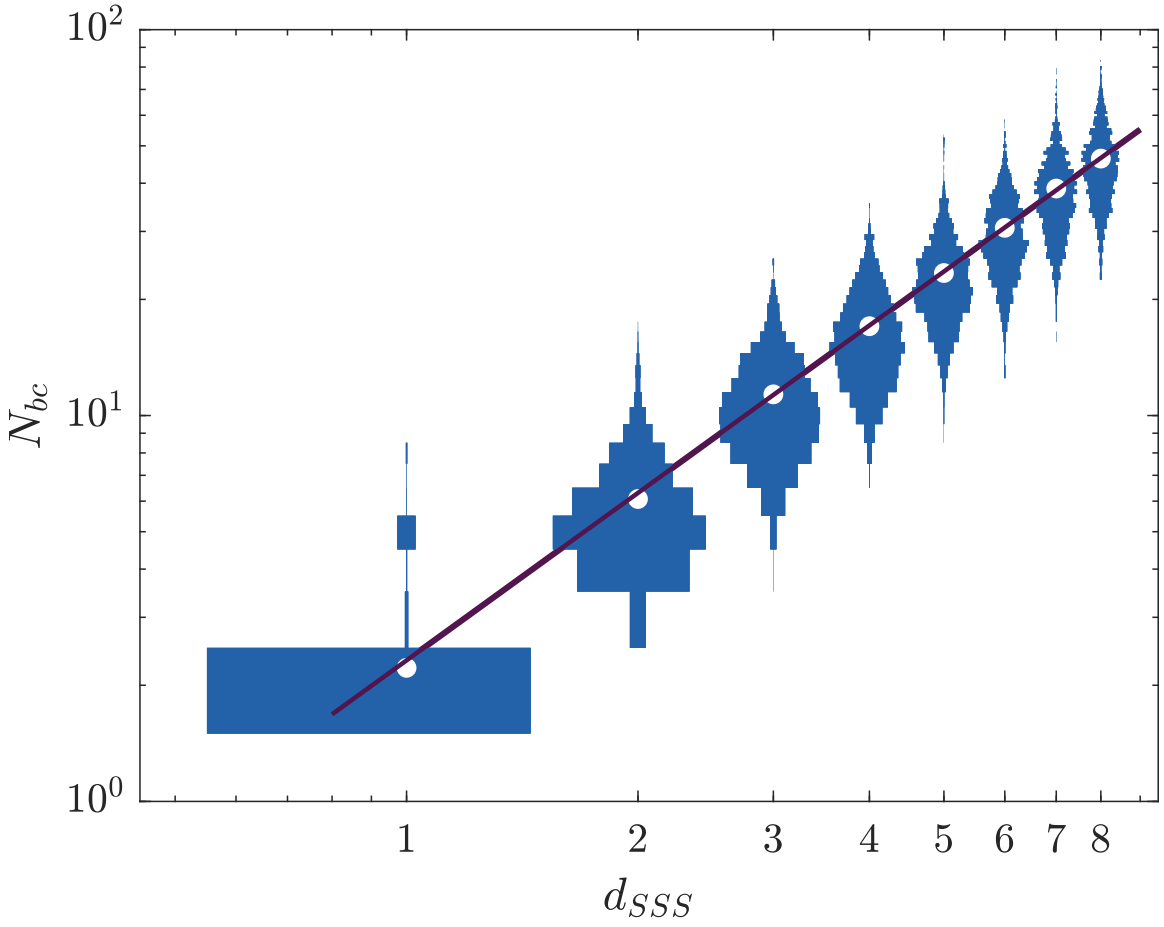

FIGURE 9. Histogram of the number of breakable contacts, N_{bc}, at each number of dimensions of the space of SSS, d_{SSS}, for $N = 128$. Purple line shows the empirical fit $N_{bc} \approx 2.43 d_{SSS}^{1.44}$.

CHAPTER IV

MEAN-FIELD PREDICTIONS OF SCALING PREFACTORS MATCH LOW-DIMENSIONAL JAMMED PACKINGS

No known analytic framework precisely explains all the phenomena observed in jamming. The replica theory for glasses and jamming is a mean-field theory which attempts to do so by working in the limit of infinite dimensions, such that correlations between neighbors are negligible. As such, results from this mean-field theory are not guaranteed to be observed in finite dimensions. However, many results in mean field for jamming have been shown to be exact or nearly exact in low dimensions. This suggests that the infinite dimensional limit is not necessary to obtain these results. In this Letter, we perform precision measurements of jamming scaling relationships between pressure, excess packing fraction, and number of excess contacts from dimensions 2–10 in order to extract the prefactors to these scalings. While these prefactors should be highly sensitive to finite dimensional corrections, we find the mean-field predictions for these prefactors to be exact in low dimensions. Thus the mean-field approximation is not necessary for deriving these prefactors. We present an exact, first-principles derivation for one, leaving the other as an open question. Our results suggest that mean-field theories of critical phenomena may compute more for $d \geq d_u$ than has been previously appreciated.

Introduction

Granular materials exhibit universal properties regardless of the material properties of the individual grains [13, 15, 35]. The jamming transition is a critical point near which properties such as pressure, packing fraction, or number of excess contacts, among others, scale as power laws. Scaling theory summarizes and condenses these power law relationships, but no first-principles theory of jammed systems at finite dimensions exists. The replica mean-field theory of glasses and jamming has been shown to be exact in the infinite dimensional limit [48, 49]. To do so it relies on the assumption that there are no correlations between neighbors, fundamentally at odds with low-dimensional systems. As such, mean-field predictions should not be expected to hold in low dimensional-jamming, and some results, most notably the packing fraction at jamming, deviate from the mean-field predictions [13, 46]. However, despite the fact that low

dimensional systems have highly correlated neighbors the scaling relations are precisely the same as those found in infinite dimensions [30, 44, 45]. Many other results predicted by the mean field have also been observed in low dimensional jamming, suggesting that they may be provable without the mean field approximation [2, 6, 12, 13, 15, 19].

Here, we move one step further in the comparison between low-dimensional jamming and mean-field jamming by probing not only scaling relations but also prefactors between a handful of properties: pressure P, excess contacts δz, and excess packing fraction above jamming $\Delta\varphi$. We demonstrate the continued success of the mean field in describing low-dimensional systems by quantitatively verifying the mean-field predictions for these prefactors. Thus, the mean-field approximation is overzealous: one need not have vanishing correlations in order to obtain these results. In this spirit we provide a first-principles proof of the relation between pressure and excess packing fraction free of the mean-field assumptions. These results call out for proofs for all of the other universal relations of the jamming transition.

Background

Granular materials undergo a jamming transition at a critical packing fraction φ_j. The number of force bearing contacts between grains jumps abruptly from zero to the minimum number sufficient to support global rigidity and thus global pressure, Z_c. In a packing of N frictionless, spherical particles in d dimensions, $Z_c = Nd + 1 - d$ [28, 35].

We limit our study to spherical particles interacting through a harmonic contact potential given by

$$U_{ij} = \varepsilon \left(1 - \frac{|\mathbf{r}_{ij}|}{\sigma_{ij}}\right)^2 \Theta\left(1 - \frac{|\mathbf{r}_{ij}|}{\sigma_{ij}}\right), \tag{4.1}$$

where ε is the energy scale, $\mathbf{r_{ij}}$ is the contact vector between particles i and j, σ_{ij} is the sum of the radii of particles i and j, and Θ is the Heaviside step function. Thus, the total energy $U = \frac{1}{2}\sum_{ij} U_{ij}$. From this potential, the forces between particles can be calculated as

$$\mathbf{f}_{ij} = \frac{2\varepsilon}{\sigma_{ij}} \left(1 - \frac{|\mathbf{r_{ij}}|}{\sigma_{ij}}\right) \Theta\left(1 - \frac{|\mathbf{r_{ij}}|}{\sigma_{ij}}\right) \hat{r}_{ij}. \tag{4.2}$$

We compute a unit and dimension independent pressure using the microscopic formula [1, 45]

$$P \equiv -\frac{\bar{V}_p}{\varepsilon}\frac{dU}{dV} = \frac{\bar{V}_p}{\varepsilon V d}\sum_{i,j}\mathbf{f}_{ij}\cdot\mathbf{r}_{ij}, \tag{4.3}$$

where V is the volume of the system and $\bar{V}_p$ is the average particle volume.

For soft spheres the packing fraction φ can be increased, leading to new contacts and an increased pressure. We thus consider three natural quantities that measure distance from jamming:

- excess packing fraction, $\Delta\varphi = \varphi - \varphi_j$
- excess contacts per particle, $\delta z = (Z - Z_c)/N$ where Z is the number of contacts
- pressure P

The relationships between these quantities are predicted by mean-field theory as [48]:

$$P = C_{p\varphi}\Delta\varphi \tag{4.4}$$

$$\delta z = C_{zp}P^{1/2} \tag{4.5}$$

with prefactors $C_{p\varphi}$ and C_{zp} which are functions only of spatial dimension [45]. These and other scaling relationships have been previously explained by approximate theories [34, 69–71] and computationally confirmed in low-dimensional jamming [28, 35, 44, 45]. They are summarized concisely by the scaling theory of the jamming transition [30]. The scaling exponents in $d \geq 2$ match those in mean field, suggesting that the transition behaves like a critical point with upper critical dimension $d_u = 2$. Moreover, mean-field theory predictions of these prefactors can be derived as [27, 48]:

$$C_{p\varphi} = \frac{1}{d}\hat{C}_{p\varphi} \tag{4.6}$$

$$C_{zp} = \frac{d}{\sqrt{2^d}}\hat{C}_{zp} \tag{4.7}$$

where $\hat{C}_{p\varphi}$ and $\hat{C}_{zp}$ are finite constants in the $d \to \infty$ limit, which have not yet been explicitly calculated. Note that these relations are presented in a particular choice of units in the literature. We include details of the conversion to our dimensionless units in the Supplemental Material. *A*

priori, it is not expected that these predictions will apply in low dimensions, in which the mean-field assumption is not warranted. Even above upper critical dimensions, mean-field theories are not generally expected to correctly compute prefactors, or even the purportedly universal amplitude ratios. Beyond scaling exponents, to our knowledge, the critical cluster shape in percolation and related phenomena [3, 51] and the Binder cumulant in the Ising model [10, 11, 47] are the only quantities which are known to be equal to their mean-field values above the upper critical dimension. Even though these prefactors for jamming scaling relationships have been measured and reported [45, 56], because they are not expected to be equal to their mean-field values they have not received substantial theoretical attention. An approximate calculation of the related prefactor between the shear modulus and number of excess contacts has been performed in three dimensions [71].

Computational methods

We use pyCudaPacking [13], a GPU-based simulation engine, to generate energy minimized soft (or penetrable) sphere packings. We do so for number of particles $N = 8192 - 32768$ and dimension $d = 2 - 10$. Our results suggest that $N = 8192$ is large enough to avoid finite size effects in $d < 9$, which we have verified in $d = 8$ by comparing our packing at $N = 8192$ with one at $N = 16384$, finding no deviation. For $d = 9$ and $d = 10$ we use system sizes of 16384 and 32768, respectively. The particles are monodisperse, except in two dimensions in which we use equal numbers of bidisperse particles with a size ratio of 1:1.4 to prevent crystallization.

The packings are subject to periodic boundary conditions. We minimize the packings using the FIRE minimization algorithm [9] using quad precision floating point numbers in order to achieve resolution on the contact network near the jamming point.

Using the same methods as described in Ref. [14], we start with randomly distributed initial positions, and apply a search algorithm to create systems approximately logarithmically spaced in $\Delta\varphi$. At each step we use the known power law relationship between energy and $\Delta\varphi$ to calculate an estimate of φ_j. We use this estimate to approximate $\Delta\varphi$ and determine the next value of φ in an effort to logarithmically space $\Delta\varphi$ values. We then adjust the packing fraction to this value of φ by uniformly scaling particle radii and minimizing the system. We continue this process until the system is nearly critically jammed, i.e. has exactly one state of self stress.

We then use the known power law relationship between pressure and $\Delta\varphi$ to fit the dataset and precisely calculate φ_j (with error less than the smallest value of $\Delta\varphi$) from which we calculate $\Delta\varphi$ at each value of φ.

Results

Figure 10 shows the measured linear scaling of pressure with packing fraction separately for each dimension. We fit the data to Eq. 4.4 to find $C_{p\varphi}$, considering only data close to jamming to avoid fitting to high pressure deviations from the scaling power law. The measured values of $C_{p\varphi}$ are shown in the inset to confirm the $1/d$ dimensional scaling predicted by mean-field theory in Eq. 4.6. A fit to this scaling provides a value of $\hat{C}_{p\varphi}$ of 1.23.

Figure 11 shows the measured square root scaling of excess contacts with pressure separately for each dimension. We fit the data to Eq. 4.5 to find C_{zp}, the values of which are shown in the inset. Beginning around three dimensions, the values of C_{zp} confirm the dimensional scaling predicted by mean-field theory in Eq. 4.7, and a fit to this scaling provides a value of $\hat{C}_{zp}$ of 0.74.

The values of both $C_{p\varphi}$ and C_{zp} are roughly consistent with values measured in previous studies [45, 56]. It has been recently suggested that the prestress, i.e., the normalized ratio of the first and second derivatives of the potential as defined in Ref. [60], is a better candidate to dedimensionalize the relationship between pressure and excess contacts. However, we find a substantially better collapse of our expected form of pressure than with prestress. For more details on prestress, see the attached Supplemental Material.

Discussion

The close agreement of our data with the mean-field predictions in low dimensions suggests that the mean-field assumption is not essential to derive these scaling and prefactor relations. In the spirit of discovering proofs for these relations free of the mean-field assumption, we expand on an earlier calculation of the bulk modulus scaling [69] to show that such a calculation can also explain the scaling of $C_{p\varphi}$ with spatial dimension and the precise value of $\hat{C}_{p\varphi}$.

From taking a derivative of Eq. 4.4, we see immediately that $C_{p\varphi}$ may be expressed in terms of the bulk modulus, $K \equiv V\frac{d^2U}{dV^2}$, at jamming:

$$C_{p\varphi} = \frac{\bar{V}_\mathrm{p} V}{\varphi\varepsilon}\frac{d^2U}{dV^2} = \frac{V}{N\varepsilon}K. \tag{4.8}$$

We note that this approximation slightly overestimates $C_{p\varphi}$: the apparently linear average stress-strain curves of jammed packings are actually the average of many piecewise linear curves with discontinuous drops in stress, thus the average slope is slightly less than the instantaneous slope [26].

At the unjamming point, the linear response of the system is that of a network of unstretched springs. Thus, at lowest order in pressure the bulk modulus is that of an unstressed spring network, which may be calculated in terms of the "states of self stress," vectors of possible spring tensions, $s \in \mathbb{R}^Z$, which do not produce any net force on a particle [36, 50, 69]. Here we explain how to carry out this calculation for a monodisperse system in the unjamming limit; a correction for polydispersity is handled in the Supplemental Material.

We begin by defining the set of "affine bond extensions," a vector $E \in \mathbb{R}^Z$ giving the amount by which each bond vector would increase under a unit volumetric expansion of the system. In linear elasticity, this simply induces an expansion of each length by $1/d$, so,

$$E_\ell = \frac{1}{d} r_\ell, \tag{4.9}$$

where we emphasize that ℓ indexes the contacts in the system rather than the particles; r_ℓ is the distance between a particular pair of particles.

In the case that all springs have the same spring constant k (e.g., monodisperse packings), the bulk modulus may be written as the projection of these affine moduli onto the states of self stress [36, 50, 69]. At jamming, there is only one state of self stress, and so the bulk modulus may be computed exactly using the projection onto only this one state of self stress [69],

$$K = \frac{k}{V}\left(\sum_{\ell=1}^{Z} s_{1,\ell} E_\ell\right)^2 \tag{4.10}$$

$$= \frac{2N\varepsilon}{dV}\frac{\langle f\rangle^2}{\langle f^2\rangle} \tag{4.11}$$

In the near jamming limit, this one special state of self stress exists all the way down to the jamming point and can be expressed in terms of the vector of physical force magnitudes, f. For the packing to be in equilibrium, this set of contact forces must produce no net force on every particle, and thus by definition the vector f is always a state of self stress. The projection defined above requires states of self stress to be normalized, and so the state of self stress may be expressed as:

$$s_{1,\ell} = \frac{1}{\sqrt{\sum_l f_l}} f_\ell = \frac{1}{\sqrt{Z\langle f^2\rangle}} f_\ell. \tag{4.12}$$

Furthermore at lowest order in P we have $r = \sigma$, and we assume $Z \approx dN$. Thus, Eq. 4.10 reduces to

$$K = \frac{Nk\sigma^2}{dV} \frac{\langle f\rangle^2}{\langle f^2\rangle} = \frac{2N\varepsilon}{dV} \frac{\langle f\rangle^2}{\langle f^2\rangle} \tag{4.13}$$

and thus via Eq. 4.8

$$C_{p\varphi} = \frac{2}{d} \frac{\langle f\rangle^2}{\langle f^2\rangle}, \tag{4.14}$$

for monodisperse spheres. The full calculation in the Supplemental Material shows that in the polydisperse case this becomes

$$C_{p\varphi} = \frac{2}{d} \frac{\langle \sigma f\rangle^2}{\langle \sigma^2 f^2\rangle}. \tag{4.15}$$

We find that the distribution of contact forces does not depend strongly on dimension, which we demonstrate and discuss in the Supplementary Material, including Refs. [14, 43]. We thus predict the scaling of $C_{p\varphi}$ to agree with the asymptotic mean-field scaling. Because this proof does not invoke the mean-field assumption, we expect this scaling to be correct in all dimensions. Moreover, we are able to calculate each value of $C_{p\varphi}$ by measuring the ratio of force distribution moments. These values are calculated as in Eq. 4.15, and are shown in Fig. 10 to precisely predict the values of $C_{p\varphi}$.

Conclusion

The mean-field theory of jamming predicts both the scaling exponents and the dimensional scaling of their prefactors. While the exponents have been previously verified, we have demonstrated that even some prefactors are well predicted in low dimensions by mean-field theory. Although these prefactors should be considered especially sensitive to finite dimensional corrections, we find the mean field prediction to be exact in low dimensions. Is this a generic phenomenon, or are the quantities we have chosen to study in this work somehow specially unaffected by finite dimensional correlations? Experience with critical phenomena suggests that although certain ratios of these prefactors (i.e. amplitude ratios) may be universal, the prefactors themselves should be both nonuniversal and challenging to compute, which has led to them being neglected. Our results demonstrate however that these prefactors may be computed exactly. These results call out for other theories of jamming and the glass transition which reproduce the mean-field results without such assumptions, or perhaps for a deeper understanding of why certain mean-field computations may be exact in finite dimensions. Additionally, our results suggest that in traditional critical phenomena mean-field theory may compute more for $d \geq d_u$ than has been previously appreciated.

Acknowledgments

We thank Francesco Zamponi for generous assistance in interpreting the mean-field results. We also thank Andrea Liu, Jim Sethna, Cam Dennis, and Aileen Carroll-Godfrey for valuable discussion and feedback. This work benefited from access to the University of Oregon high performance computer, Talapas. This work was supported by National Science Foundation (NSF) Career Grant No. DMR-1255370 and the Simons Foundation No. 454939 (J.D.S. and E.I.C.) and by an NSERC PGS-D fellowship and Simons Foundation No. 454945 to Andrea J. Liu. (S.A.R.).

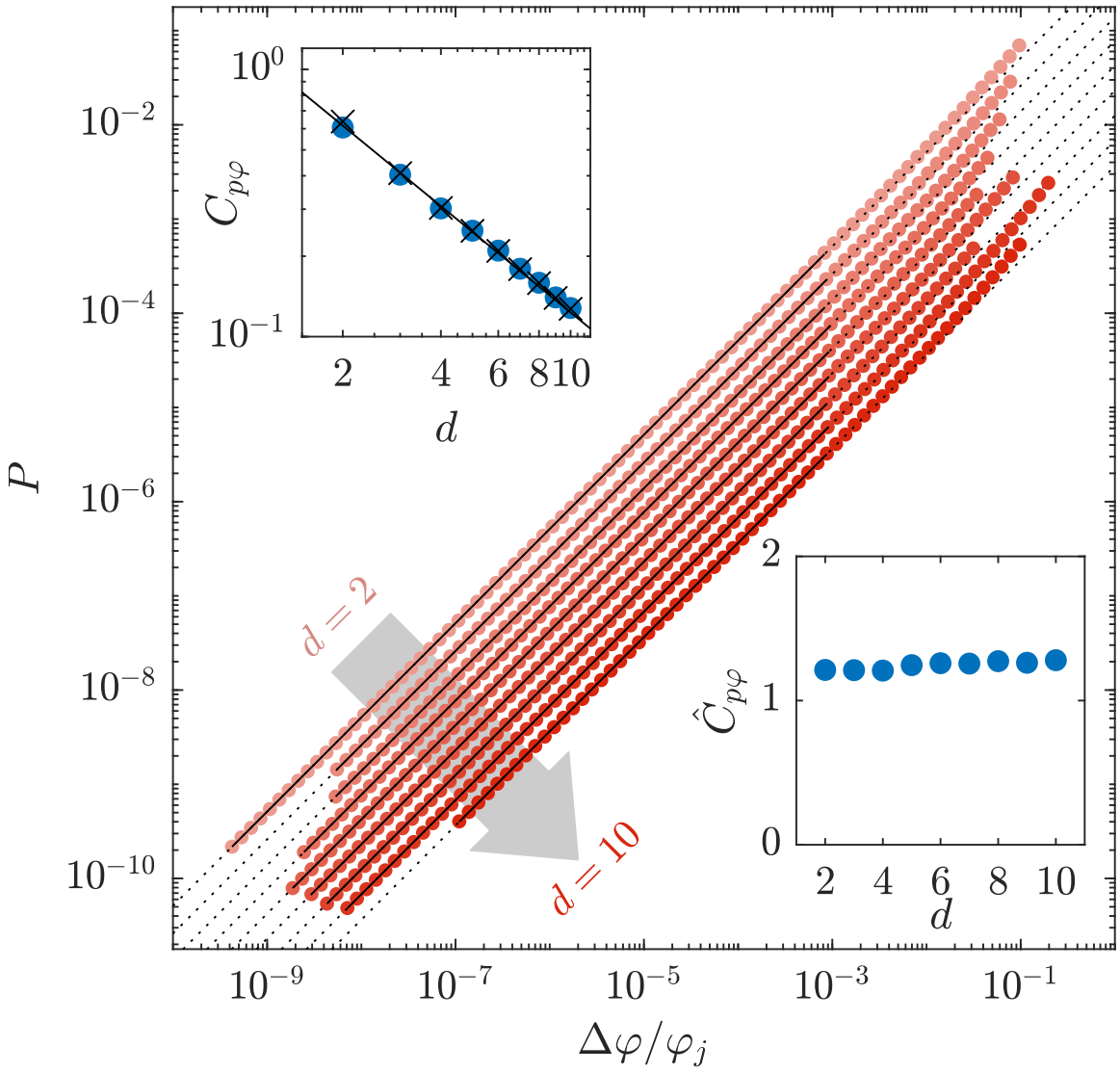

FIGURE 10. Measured pressure scales linearly with scaled excess packing fraction for systems from $d = 2$ to $d = 10$. Measured values for φ_j in our protocol are included in the Supplemental Material. Black lines show fits for $C_{p\varphi}$ using Eq. 4.4. We exclude from the fit data with $\Delta\varphi/\varphi_j > 10^{-3}$, to avoid the effect of larger overlaps causing deviations from this power law. Dotted lines show the extension of fits beyond fitted range. Upper inset shows the measured values of $C_{p\varphi}$ (blue circles) to scale in agreement with the mean-field prediction Eq. 4.6, shown as a fit to a black line with $\hat{C}_{p\varphi} \approx 1.23$. Moreover, they are in precise agreement with predicted values from Eq. 4.15 (marked with black $\times$'s). Lower inset shows measured values of $\hat{C}_{p\varphi}$ calculated from the measured values of $C_{p\varphi}$ and eqn 4.6. While each prefactor is measured from a single system, the prefactors for a second, identically constructed dataset were calculated to be well within the bounds of the marker size.

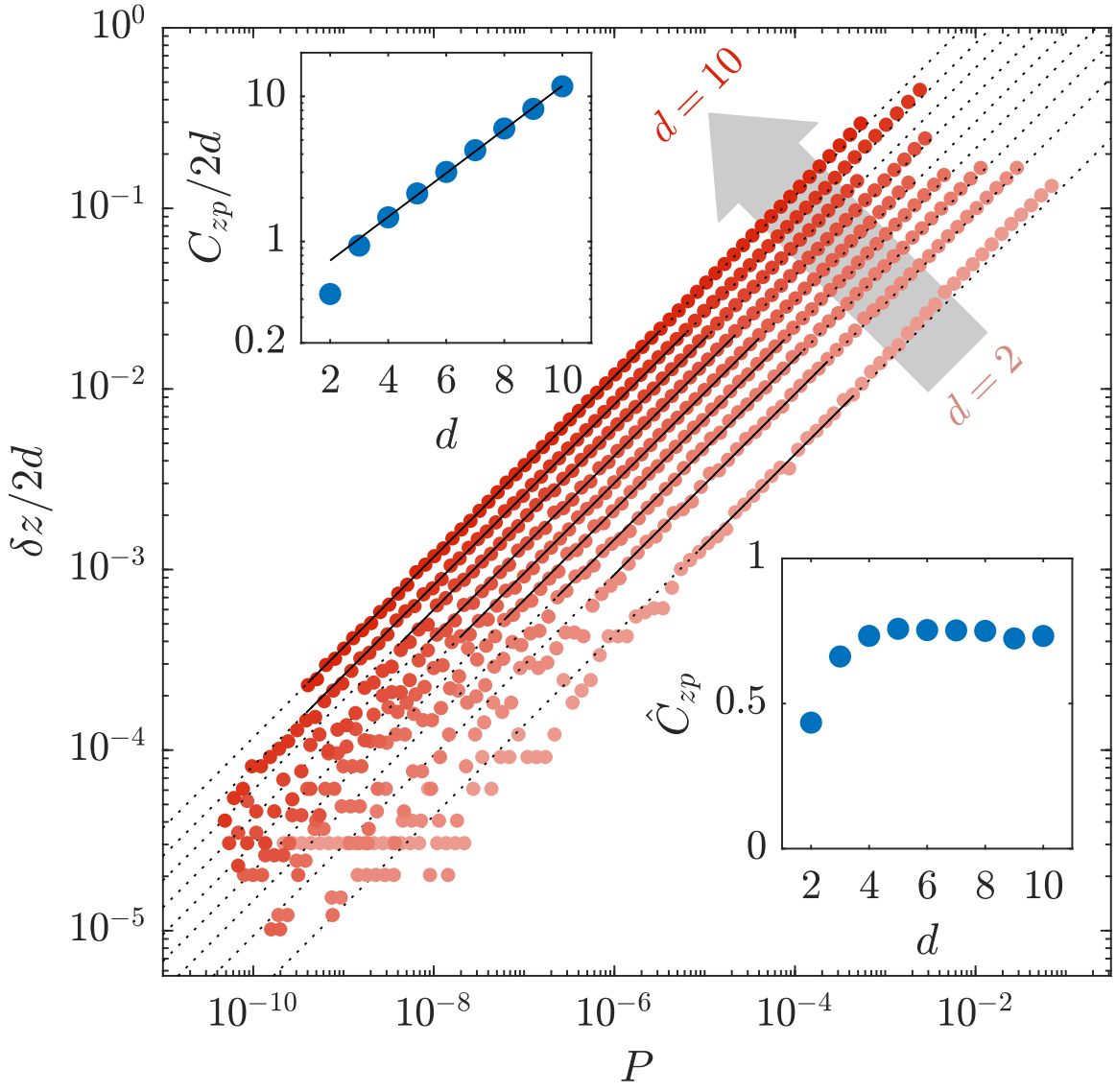

FIGURE 11. Measured excess contacts scales with the square root of pressure for systems from $d = 2$ to $d = 10$. Black lines show fits for C_{zp} using Eq. 4.5. For our fits, we ignore high pressure data as in Fig. 10, and additionally exclude data with less than 40 excess contacts to avoid fitting to small number fluctuations. Dotted lines show the extension of our fits beyond fitted range. Lower inset shows the measured values of C_{zp} (blue circles), which scale in agreement with the mean-field prediction Eq. 4.7, shown as a fit to a black line and with $\hat{C}_{zp} \approx 0.74$. Upper inset shows measured values of $\hat{C}_{zp}$ calculated from the measured values of C_{zp} and Eq. 4.7. While each prefactor is measured from a single system, the prefactors for a second, identically constructed dataset were calculated to be well within the bounds of the marker size.

Supplementary Material of "Mean-field predictions of scaling prefactors match low-dimensional jammed packings"

Measured values of φ_j

In Table 1 we show our measued values of φ_j. these values are used in calculating $\Delta\varphi$.

TABLE 1. Measured values of φ_j in dimensions 2-10.

d	2	3	4	5	6	7	8	9	10
φ_j	0.85	0.65	0.46	0.31	0.20	0.13	0.078	0.049	0.029

Mean Field Prediction of Pressure vs Packing Fraction

Mean field theory predicts that pressure scales with packing fraction as follows [48]:

$$\hat{P} = \hat{C}(\hat{\varphi} - \hat{\varphi}_j) \tag{4.16}$$

where $\hat{C}_{p\varphi}$ is a constant, and the hats over P and $\Delta\varphi$ signify that the quantities are scaled such to be fixed in the infinite dimensional limit, as follows:

$$\hat{P} = \frac{P^*}{\rho d} \tag{4.17}$$

$$\hat{\varphi} = \frac{2^d}{d}\varphi \tag{4.18}$$

where ρ is the number density, $\frac{N}{V}$, and P^* is the pressure which is calculated with assumed unit particle diameter. This relates to our pressure, P, as follows:

$$P = \frac{\varphi}{\rho}\frac{1}{d^2}P^*, \tag{4.19}$$

where the factor of $\frac{\varphi}{\rho}$ unwraps their assumption of unit particle diameter, and the factor of $\frac{1}{d^2}$ comes from their potential, which explicitly contains a dimensional term:

$$U^*(r) = \frac{\epsilon d^2}{2}\left(\frac{r}{\ell} - 1\right)^2 \Theta\left(\ell - r\right). \tag{4.20}$$

We can thus rewrite equation 4.17 in terms of our pressure P:

$$\hat{P} = \frac{d}{\varphi} P, \tag{4.21}$$

and therefore equation 4.16:

$$\frac{d}{\varphi} P = \hat{C} \frac{2^d}{d} (\varphi - \varphi_j) \tag{4.22}$$

$$P = \frac{\varphi}{d} \hat{C} \frac{2^d}{d} \Delta\varphi \tag{4.23}$$

$$P = \frac{1}{d} \hat{C} \hat{\varphi}_j (\Delta\varphi) \tag{4.24}$$

$$P = \frac{1}{d} \hat{C}_{p\varphi} (\Delta\varphi). \tag{4.25}$$

Where, noting that $\hat{\varphi}_j$ and $\hat{C}$ are constants in the infinite dimensional limit, we combine them as $\hat{C}_{p\varphi}$. Thus mean field predicts a simple $1/d$ scaling of the prefactor between pressure and excess packing fraction.

Mean Field Prediction of Pressure vs Number Of Excess Contacts

The number of contacts, z, is predicted by mean field theory to have the form [48]:

$$\frac{z}{2d} = 1 + \hat{C}_{z\varphi} \sqrt{\hat{\varphi} - \hat{\varphi_j}} \tag{4.26}$$

$$\frac{z}{2d} = 1 + \hat{C}_{z\varphi} \sqrt{\frac{2^d}{d}} \sqrt{\varphi - \varphi_j} \tag{4.27}$$

for some constant $\hat{C}_{z\varphi}$.

The number of excess contacts, δz, therefore is predicted to scale as follows:

$$\frac{\delta z}{2d} = \hat{C}_{z\varphi} \sqrt{\frac{2^d}{d}} \sqrt{\varphi - \varphi_j} \tag{4.28}$$

$$\delta z = 2d \hat{C}_{z\varphi} \sqrt{\frac{2^d}{d}} \sqrt{\varphi - \varphi_j}. \tag{4.29}$$

By combining equations 4.25 and 4.29, we can also predict the relation between δz and P:

$$\delta z = 2d\hat{C}_{z\varphi}\sqrt{\frac{2^d}{d}}\sqrt{\frac{d}{\hat{C}_{p\varphi}}P} \tag{4.30}$$

$$= 2d\hat{C}_{z\varphi}\sqrt{\frac{2^d}{\hat{C}_{p\varphi}}}\sqrt{P} \tag{4.31}$$

$$\tag{4.32}$$

where we define $\hat{C}_{zp} = \frac{2\hat{C}_{z\varphi}}{\sqrt{\hat{C}_{p\varphi}}}$.

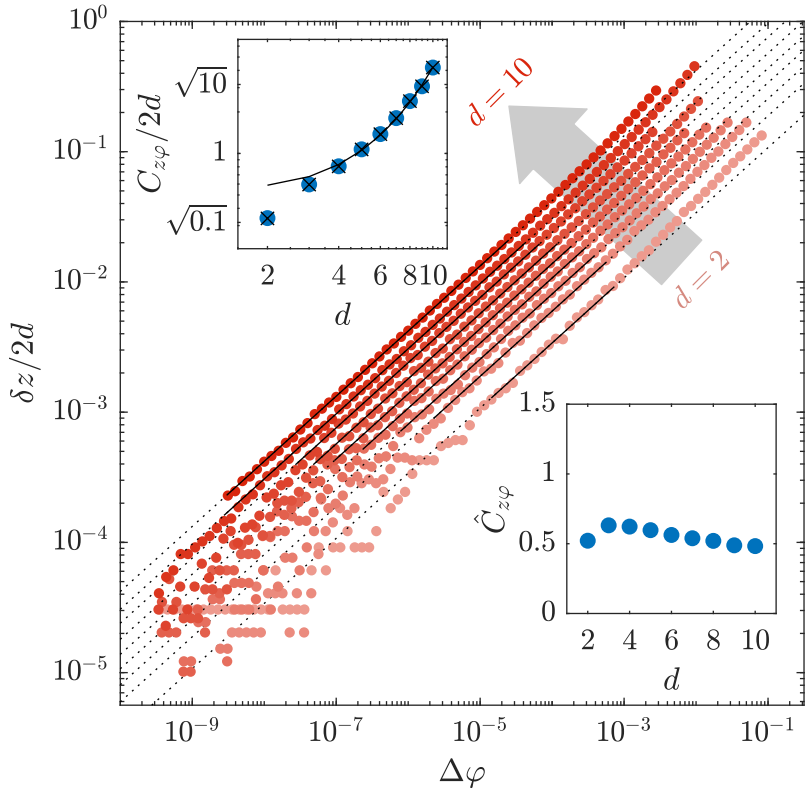

FIGURE 12. Measured excess contacts scales with the square root of excess packing fraction for systems from $d = 2$ to $d = 10$ (red circles). Black lines show the fits for C_{zp} using eqn 4.33. For our fits, we ignore data at high pressure and low contact number as in figure 11. Dotted lines show the extension of our fits beyond the fitted range. Inset shows the measured values of $C_{z\varphi}$ (blue circles), which scale in agreement with the mean field prediction eqn 4.29 using measured values of with $\hat{C}_{z\varphi} \approx 0.83$. Additionally, to note consistency we show that our measured values of $C_{z\varphi}$ agree well with values calculated from our measurements of $C_{p\varphi}$ and C_{zp} using eqn 4.34 (black x's).

Excess Contacts vs Excess Packing Fraction Prefactor Scaling

From eqns 4.4 and 4.5 we can simply relate δz and φ as follows:

$$\delta z = C_{z\varphi} \left(\Delta\varphi\right)^{1/2} \tag{4.33}$$

where clearly,

$$C_{z\varphi} = C_{zp}\sqrt{C_{p\varphi}}. \tag{4.34}$$

In figure 12, we show this scaling seperately for each dimension. We fit each line to eqn 4.33 to find the values of the prefactor $C_{z\varphi}$ in each dimension, the values of which are shown in the inset. These values agree well with both the mean field prediction above $3D$, shown as a black line, and our calculated value from C_{zp} and $C_{p\varphi}$, shown as black x's in figures 10 and 11.

Dimensional Dependence of Force Moment Ratios

In figure 13 we show that the ratio of force moments does not depend strongly on dimension. This empirical fact may seem at odds with previous reports of how the low-force part of the distribution differs from its mean-field form in low dimensions [14, 43]. The low-force part of the distribution has $P(f) \propto f^{\theta}$, where $\theta \approx 0.17$ in $d = 2$ smoothly rises to a $d = \infty$ value of $\theta \approx 0.42$. The high-force behaviour decays like an exponential or a stretched exponential; thus, we have computed the theoretical value of this moment ratio for distributions of the form $P(f) \sim f^{\theta}e^{-f/f_0}$ and $P(f) \sim f^{\theta}e^{-f^2/f_0^2}$, as shown in figure 14. We find that neither of these assumed distributions quantitatively predicts the measured moment ratio for the known values of θ, but they do show that the known variation in θ should not make us expect a large variation in this moment ratio.

Accounting for Polydispersity in Pressure vs. Packing Fraction Scaling

To account for the case with varying spring constants we also form the matrix of inverse spring constants

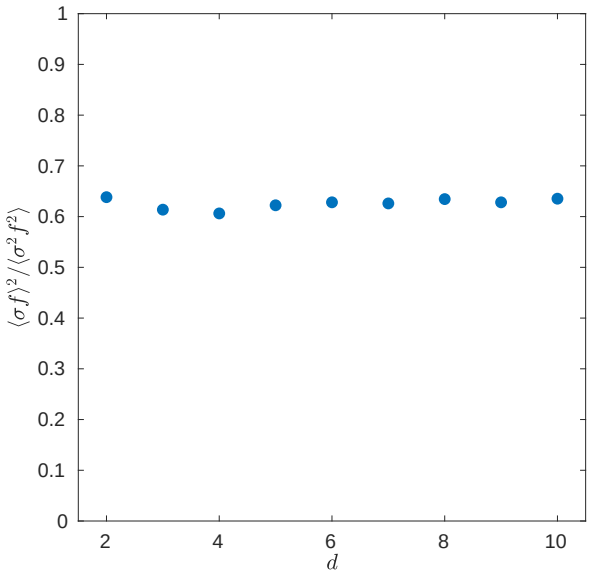

FIGURE 13. Dimensionless moment ratio of first and second moments of σf shows no dimensional dependence

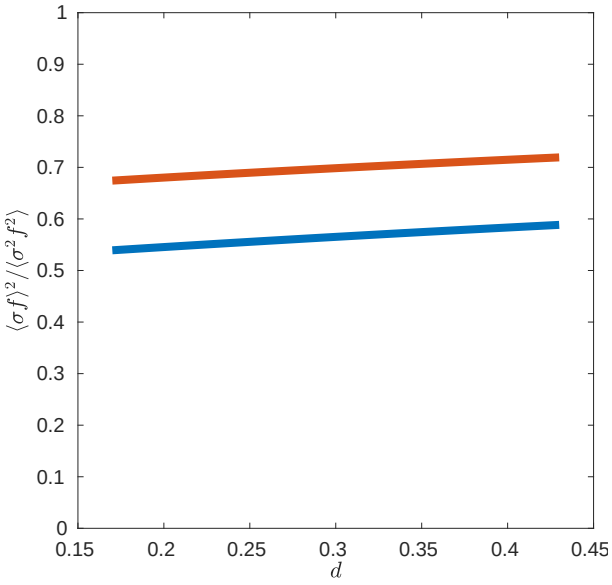

FIGURE 14. Neither the force distribution $f^\theta e^{-f/f_0}$ (blue) nor the distribution $f^\theta e^{-f^2/f_0^2}$ (red) predicts a strong θ dependence for the relevant moment ratio

$$k^{-1} = \frac{1}{2\varepsilon}\begin{pmatrix} \sigma_{ij}^2 & & \\ & \ddots & \\ & & \sigma_{kl}^2 \end{pmatrix}. \tag{4.35}$$

and the projection operator onto the states of self stress

$$S = \sum_{i=1}^{N\Delta z} |s_i\rangle \langle s_i| . \tag{4.36}$$

In terms of these quantities, the bulk modulus may be written as [36, 50, 69]

$$\frac{\partial^2 E}{\partial V^2} = \frac{1}{V} \langle E| S \left(S \left(k^{-1} \right) S \right)^{-1} S |E\rangle . \tag{4.37}$$

In the one SSS approximation, we can evaluate the two projected quantities that we need to evaluate equation 4.37. Equations 4.9 and 4.12 give

$$S |E\rangle = \langle s_0|f\rangle |s_0\rangle = \frac{\langle r|f\rangle}{d\sqrt{\langle f|f\rangle}} |s_0\rangle = \sqrt{Z} \frac{\langle rf\rangle}{d\sqrt{\langle f^2\rangle}} |s_0\rangle , \tag{4.38}$$

and equations 4.35 and 4.12 give

$$Sk^{-1}S = |s_0\rangle \langle s_0|k^{-1}|s_0\rangle \langle s_0| = |s_0\rangle \frac{\langle \sigma^2 f^2\rangle}{2\epsilon\langle f^2\rangle} \langle s_0| \tag{4.39}$$

$$\left(Sk^{-1}S\right)^{-1} = |s_0\rangle \frac{2\epsilon\langle f^2\rangle}{\langle \sigma^2 f^2\rangle} \langle s_0| \tag{4.40}$$

Furthermore at lowest order in P we have $|r\rangle = |\sigma\rangle$, and we may assume $Z \approx dN$. Thus, equation 4.37 reduces to

$$K = \frac{2N\varepsilon}{dV} \frac{\langle \sigma f\rangle^2}{\langle \sigma^2 f^2\rangle}, \tag{4.41}$$

and thus via equation 4.8:

$$C_{p\varphi} = \frac{2}{d} \frac{\langle \sigma f\rangle^2}{\langle \sigma^2 f^2\rangle}. \tag{4.42}$$

Prestress Comparison

It has recently been suggested the relationship between prestress and number of excess contacts collapses perfectly when compared across dimensions [60]. We define prestress e as in ref.

[60] as:

$$e = (d-1)\left\langle \frac{-V'(r_{ij})}{r_{ij}V''(r_{ij}} \right\rangle_{ij} \tag{4.43}$$

and expected to scale as:

$$\delta z = C_{ze} e^{\frac{1}{2}} \tag{4.44}$$

because it is proportional to pressure near the jamming transition [60]. In figures 16 and 15,, we examine the collapse of scaled excess contacts with prestress and compare it to the collapse of excess contacts scaled by the mean field prediction with pressure. In figure 16 we see that the collapse with prestress is not quite perfect - there is a clear upward trend. This stands in contrast to the inset of figure 15, which shows $\hat{C}_{zp}$ to be nearly constant above three dimensions.

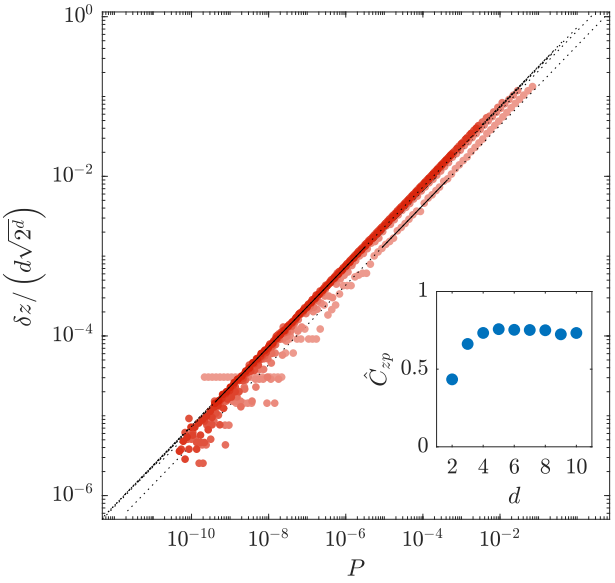

FIGURE 15. Scaled excess contacts scales with the square root of pressure as in figure 11. However, with excess contacts scaled by the expected mean field prediction, eqn. 4.7, the data collapse onto a single line. The inset confirms the collapse, showing $\hat{C}_{zp}$ to be nearly constant.

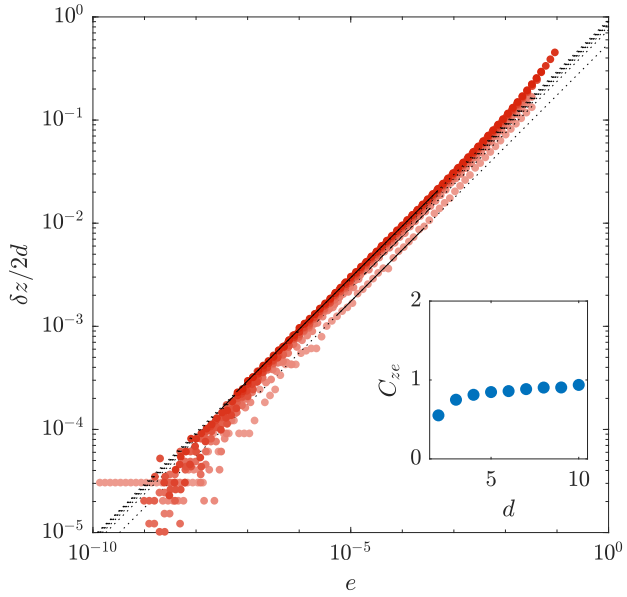

FIGURE 16. Scaled excess contacts scales with the square root of prestress for systems from $d = 2$ to $d = 10$. Black lines show the fits for C_{ze} using eqn 4.44. The fits ignore high and low pressure data as in figure 11. Lower inset shows the measured values of C_{ze} which have a clear upward trend.

In fact, close to jamming so that $r \approx \sigma$ and $Z \approx Nd$, our dimensionless pressure P as defined in equation 4.3 is related to the prestress by

$$P = \frac{\bar{V}_p}{\varepsilon V d} \sum_{i,j} \mathbf{f}_{ij} \cdot \mathbf{r}_{ij} \tag{4.45}$$

$$= \frac{\bar{V}_p}{\varepsilon V d} Z \langle f_{ij} r_{ij} \rangle_{ij} \tag{4.46}$$

$$= \frac{2\varphi Z}{d} \left\langle \frac{r_{ij}}{\sigma_{ij}} \left(1 - \frac{r_{ij}}{\sigma_i j} \right) \right\rangle_{ij} \tag{4.47}$$

$$= \frac{2\varphi Z}{d} \left\langle \frac{-r_{ij} V'(r_{ij})}{\sigma_{ij}^2 V''(r_{ij}} \right\rangle_{ij} \tag{4.48}$$

$$\approx 2 \frac{\varphi_{\mathrm{J}}}{d-1} e. \tag{4.49}$$

Thus, our better-fitting form for the $z - P$ relationship amounts to the statement that

$$\frac{\Delta z}{2d} = \hat{C}_\varphi \sqrt{\frac{d}{d-1}} \sqrt{e}. \tag{4.50}$$

Thus our scaling forms agree with the statement of reference [60] in the infinite-d limit, although we see better fit with our form in low dimensions.

CHAPTER V

CONCLUSION

we did a pretty good job on all this, don't you think?

REFERENCES CITED

[1] Allen, M. P., Allen, M. P., Tildesley, D. J., ALLEN, T., and Tildesley, D. J. (1989). *Computer Simulation of Liquids*. Clarendon Press.

[2] Arceri, F. and Corwin, E. I. (2019). Vibrational properties of hard and soft spheres are unified at jamming. *arXiv:1912.05697 [cond-mat]*. arXiv: 1912.05697.

[3] Aronovitz, J. A. and Stephen, M. J. (1987). Universal features of the shapes of percolation clusters and lattice animals. *Journal of Physics A: Mathematical and General*, 20(9):2539–2556.

[4] Barber, C. B., Dobkin, D. P., and Huhdanpaa, H. (1996). The quickhull algorithm for convex hulls. *ACM Transactions on Mathematical Software*, 22(4):469–483.

[5] Bennett, C. H. (1976). Efficient estimation of free energy differences from Monte Carlo data. *Journal of Computational Physics*, 22(2):245–268.

[6] Berthier, L., Biroli, G., Charbonneau, P., Corwin, E. I., Franz, S., and Zamponi, F. (2019). Perspective: Gardner Physics in Amorphous Solids and Beyond. *The Journal of Chemical Physics*, 151(1):010901. arXiv: 1902.10494.

[7] Bi, D., Henkes, S., Daniels, K. E., and Chakraborty, B. (2015). The Statistical Physics of Athermal Materials. *Annual Review of Condensed Matter Physics*, 6(1):63–83. arXiv: 1404.1854.

[8] Bililign, E. S., Kollmer, J. E., and Daniels, K. E. (2019). Protocol Dependence and State Variables in the Force-Moment Ensemble. *Physical Review Letters*, 122(3):038001.

[9] Bitzek, E., Koskinen, P., Gähler, F., Moseler, M., and Gumbsch, P. (2006). Structural Relaxation Made Simple. *Physical Review Letters*, 97(17).

[10] Blöte, H. W. J. and Luijten, E. (1997). Universality and the five-dimensional Ising model. *Europhysics Letters (EPL)*, 38(8):565–570.

[11] Brizin, E. and Zinn-Justin, J. (1985). Finite size effects in phase transitions. *Nuclear Physics B*, 257:27.

[12] Charbonneau, P., Corwin, E. I., Parisi, G., Poncet, A., and Zamponi, F. (2016). Universal Non-Debye Scaling in the Density of States of Amorphous Solids. *Physical Review Letters*, 117(4).

[13] Charbonneau, P., Corwin, E. I., Parisi, G., and Zamponi, F. (2012). Universal Microstructure and Mechanical Stability of Jammed Packings. *Physical Review Letters*, 109(20).

[14] Charbonneau, P., Corwin, E. I., Parisi, G., and Zamponi, F. (2015). Jamming Criticality Revealed by Removing Localized Buckling Excitations. *Physical Review Letters*, 114(12). arXiv: 1411.3975.

[15] Charbonneau, P., Kurchan, J., Parisi, G., Urbani, P., and Zamponi, F. (2017). Glass and Jamming Transitions: From Exact Results to Finite-Dimensional Descriptions. *Annual Review of Condensed Matter Physics*, 8(1):265–288.

[16] Cubuk, E., Schoenholz, S., Rieser, J., Malone, B., Rottler, J., Durian, D., Kaxiras, E., and Liu, A. (2015). Identifying Structural Flow Defects in Disordered Solids Using Machine-Learning Methods. *Physical Review Letters*, 114(10):108001.

[17] Cubuk, E. D., Schoenholz, S. S., Kaxiras, E., and Liu, A. J. (2016). Structural Properties of Defects in Glassy Liquids. *The Journal of Physical Chemistry B*, 120(26):6139–6146.

[18] Dagois-Bohy, S., Tighe, B. P., Simon, J., Henkes, S., and van Hecke, M. (2012). Soft-Sphere Packings at Finite Pressure but Unstable to Shear. *Physical Review Letters*, 109(9).

[19] Dennis, R. and Corwin, E. (2020). Jamming Energy Landscape is Hierarchical and Ultrametric. *Physical Review Letters*, 124(7).

[20] Ding, J., Patinet, S., Falk, M. L., Cheng, Y., and Ma, E. (2014). Soft spots and their structural signature in a metallic glass. *Proceedings of the National Academy of Sciences*, 111(39):14052–14056.

[21] Edwards, S. and Oakeshott, R. (1989). Theory of powders. *Physica A: Statistical Mechanics and its Applications*, 157(3):1080–1090.

[22] Edwards, S. F. (2008). The distribution of forces in a granular system under external stress is a spinglass problem. *Journal of Physics A: Mathematical and Theoretical*, 41(32):324019.

[23] Edwards, S. F. and Grinev, D. V. (2002). Granular materials: Towards the statistical mechanics of jammed configurations. *Advances in Physics*, 51(8):1669–1684.

[24] Ellenbroek, W. G., Hagh, V. F., Kumar, A., Thorpe, M., and van Hecke, M. (2015). Rigidity Loss in Disordered Systems: Three Scenarios. *Physical Review Letters*, 114(13).

[25] F. Hagh, V., Corwin, E. I., Stephenson, K., and Thorpe, M. F. (2019). A broader view on jamming: from spring networks to circle packings. *Soft Matter*, 15(15):3076–3084.

[26] Fan, M., Zhang, K., Schroers, J., Shattuck, M. D., and O'Hern, C. S. (2017). Particle rearrangement and softening contributions to the nonlinear mechanical response of glasses. *Physical Review E*, 96(3).

[27] Franz, S., Parisi, G., Sevelev, M., Urbani, P., and Zamponi, F. (2017). Universality of the SAT-UNSAT (jamming) threshold in non-convex continuous constraint satisfaction problems. *SciPost Physics*, 2(3).

[28] Goodrich, C. P., Liu, A. J., and Nagel, S. R. (2012). Finite-Size Scaling at the Jamming Transition. *Physical Review Letters*, 109(9).

[29] Goodrich, C. P., Liu, A. J., and Nagel, S. R. (2014). Solids between the mechanical extremes of order and disorder. *Nature Physics*, 10(8):578–581.

[30] Goodrich, C. P., Liu, A. J., and Sethna, J. P. (2016). Scaling ansatz for the jamming transition. *Proceedings of the National Academy of Sciences*, 113(35):9745–9750.

[31] Grimus, W. (2013). 100th anniversary of the Sackur–Tetrode equation. *Annalen der Physik*, 525(3):A32–A35.

[32] Henkes, S. and Chakraborty, B. (2009). A statistical mechanics framework for static granular matter. *Physical Review E*, 79(6). arXiv: 0810.5715.

[33] Jordan, C. (1875). Essai sur la géométrie à n dimensions. *Bulletin de la Société mathématique de France*, 2:103–174.

[34] Liarte, D. B., Mao, X., Stenull, O., and Lubensky, T. (2019). Jamming as a Multicritical Point. *Physical Review Letters*, 122(12).

[35] Liu, A. J. and Nagel, S. R. (2010). The Jamming Transition and the Marginally Jammed Solid. *Annual Review of Condensed Matter Physics*, 1(1):347–369.

[36] Lubensky, T. C., Kane, C. L., Mao, X., Souslov, A., and Sun, K. (2015). Phonons and elasticity in critically coordinated lattices. *Reports on Progress in Physics*, 78(7):073901.

[37] Mailman, M. and Chakraborty, B. (2012). Using point-to-set correlations to probe unjamming of frictionless grains. *Journal of Statistical Mechanics-theory and Experiment - J STAT MECH-THEORY EXP*, 2012.

[38] Manning, M. L. and Liu, A. J. (2011). Vibrational Modes Identify Soft Spots in a Sheared Disordered Packing. *Physical Review Letters*, 107(10):108302.

[39] Maxwell, J. C. (1864). On the calculation of the equilibrium and stiffness of frames. *The London, Edinburgh, and Dublin Philosophical Magazine and Journal of Science*, 27(182):294–299.

[40] McNamara, S., Richard, P., de Richter, S. K., Le Caër, G., and Delannay, R. (2009). Measurement of granular entropy. *Physical Review E*, 80(3).

[41] Morse, P., Wijtmans, S., van Deen, M., van Hecke, M., and Manning, M. L. (2020). Differences in plasticity between hard and soft spheres. *Physical Review Research*, 2(2):023179.

[42] Morse, P. K. and Corwin, E. I. (2017). Echoes of the Glass Transition in Athermal Soft Spheres. *Physical Review Letters*, 119(11):118003.

[43] Mueth, D. M., Jaeger, H. M., and Nagel, S. R. (1998). Force distribution in a granular medium. *Physical Review E*, 57(3):3164–3169.

[44] O'Hern, C. S., Langer, S. A., Liu, A. J., and Nagel, S. R. (2002). Random Packings of Frictionless Particles. *Physical Review Letters*, 88(7).

[45] O'Hern, C. S., Silbert, L. E., Liu, A. J., and Nagel, S. R. (2003). Jamming at zero temperature and zero applied stress: The epitome of disorder. *Physical Review E*, 68(1).

[46] Parisi, G., Pollack, Y. G., Procaccia, I., Rainone, C., and Singh, M. (2018). Robustness of mean field theory for hard sphere models. *Physical Review E*, 97(6).

[47] Parisi, G. and Ruiz-Lorenzo, J. J. (1996). Scaling above the upper critical dimension in Ising models. *Physical Review B*, 54(6):R3698–R3701.

[48] Parisi, G., Urbani, P., and Zamponi, F. (2020). *Theory of Simple Glasses: Exact Solutions in Infinite Dimensions*. Cambridge University Press, New York.

[49] Parisi, G. and Zamponi, F. (2010). Mean-field theory of hard sphere glasses and jamming. *Reviews of Modern Physics*, 82(1):789–845.

[50] Pellegrino, S. (1993). Structural computations with the singular value decomposition of the equilibrium matrix. *International Journal of Solids and Structures*, 30(21):3025–3035.

[51] Privman, V., Hohenberg, P. C., and Aharony, A. (1991). *Universal Critical-Point Amplitude Relations, in "Phase transition and critical phenomena" vol. 14, C. Domb and JL Lebowitz eds.* Academic Press.

[52] Puckett, J. G. and Daniels, K. E. (2013). Equilibrating Temperaturelike Variables in Jammed Granular Subsystems. *Physical Review Letters*, 110(5):058001.

[53] Richard, D., Ozawa, M., Patinet, S., Stanifer, E., Shang, B., Ridout, S. A., Xu, B., Zhang, G., Morse, P. K., Barrat, J.-L., Berthier, L., Falk, M. L., Guan, P., Liu, A. J., Martens, K., Sastry, S., Vandembroucq, D., Lerner, E., and Manning, M. L. (2020). Predicting plasticity in disordered solids from structural indicators. *Physical Review Materials*, 4(11):113609.

[54] Ridout, S. A., Rocks, J. W., and Liu, A. J. (2020). Correlation of plastic events with local structure in jammed packings across spatial dimensions. *arXiv:2011.13049 [cond-mat]*. arXiv: 2011.13049.

[55] Rocks, J. W., Ridout, S. A., and Liu, A. J. (2021). Learning-based approach to plasticity in athermal sheared amorphous packings: Improving softness. *APL Materials*, 9(2):021107.

[56] Sartor, J. D. and Corwin, E. I. (2020). Direct measurement of force configurational entropy in jamming. *Physical Review E*, 101(5).

[57] Sartor, J. D., Ridout, S. A., and Corwin, E. I. (2021). Mean-Field Predictions of Scaling Prefactors Match Low-Dimensional Jammed Packings. *Physical Review Letters*, 126(4):048001.

[58] Schoenholz, S. S., Cubuk, E. D., Sussman, D. M., Kaxiras, E., and Liu, A. J. (2016). A structural approach to relaxation in glassy liquids. *Nature Physics*, 12(5):469–471.

[59] Schoenholz, S. S., Liu, A. J., Riggleman, R. A., and Rottler, J. (2014). Understanding Plastic Deformation in Thermal Glasses from Single-Soft-Spot Dynamics. page 11.

[60] Shimada, M., Mizuno, H., Berthier, L., and Ikeda, A. (2019). Low-frequency vibrations of jammed packings in large spatial dimensions. *arXiv:1910.07238 [cond-mat]*. arXiv: 1910.07238.

[61] Snoeijer, J. H., Vlugt, T. J. H., van Hecke, M., and van Saarloos, W. (2004). Force Network Ensemble: A New Approach to Static Granular Matter. *Physical Review Letters*, 92(5).

[62] Sussman, D. M., Goodrich, C. P., and Liu, A. J. (2016). Spatial structure of states of self stress in jammed systems. *Soft Matter*, 12(17):3982–3990.

[63] Taylor, G. (1934). The mechanism of plastic deformation of crystals. Part I.—Theoretical. *Proceedings of the Royal Society of London. Series A, Containing Papers of a Mathematical and Physical Character*, 145(855):362–387.

[64] Tetrode, H. (1912). Die chemische Konstante der Gase und das elementare Wirkungsquantum. *Annalen der Physik*, 343(7):434–442.

[65] Tighe, B. P., Snoeijer, J. H., Vlugt, T. J. H., and van Hecke, M. (2010). The force network ensemble for granular packings. *Soft Matter*, 6(13):2908.

[66] Tighe, B. P. and Vlugt, T. J. H. (2011). Stress fluctuations in granular force networks. *Journal of Statistical Mechanics: Theory and Experiment*, 2011(04):P04002.

[67] Tuckman, P. J., VanderWerf, K., Yuan, Y., Zhang, S., Zhang, J., Shattuck, M. D., and O'Hern, C. S. (2020). Contact network changes in ordered and disordered disk packings. *Soft Matter*, 16(41):9443–9455.

[68] Wijtmans, S. and Manning, M. L. (2017). Disentangling defects and sound modes in disordered solids. *Soft Matter*, 13(34):5649–5655.

[69] Wyart, M. (2005). On the rigidity of amorphous solids. *Annales de Physique*, 30(3):1–96.

[70] Wyart, M., Silbert, L. E., Nagel, S. R., and Witten, T. A. (2005). Effects of compression on the vibrational modes of marginally jammed solids. *Physical Review E*, 72(5).

[71] Zaccone, A. and Scossa-Romano, E. (2011). Approximate analytical description of the nonaffine response of amorphous solids. *Physical Review B*, 83(18).